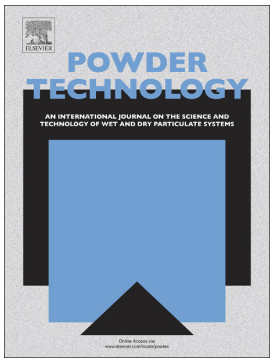

Formulation, spray drying and physico-chemical characterization of functional powders loaded with chia seed oil and prepared by complex coacervation

M. Gabriela Bordón, Alejandro J. Paredes, Nahuel M. Camacho, M. Cecilia Penci, Agustín González, Santiago D. Palma, Pablo D. Ribotta, Marcela L. Martinez

PII: S0032-5910(21)00559-3

DOI: https://doi.org/10.1016/j.powtec.2021.06.035

Reference: PTEC 16600

To appear in: *Powder Technology*

Please cite this article as: M.G. Bordón, A.J. Paredes, N.M. Camacho, et al., Formulation, spray drying and physico-chemical characterization of functional powders loaded with chia seed oil and prepared by complex coacervation, *Powder Technology* (2021), https://doi.org/10.1016/j.powtec.2021.06.035

Formulation, spray drying and physico-chemical characterization of functional powders loaded with chia seed oil and prepared by complex coacervation

M. Gabriela Bordón[1,2], Alejandro J. Paredes[5,7], Nahuel M. Camacho[5], M. Cecilia Penci[1,2,3], Agustín González[6], Santiago D. Palma[5], Pablo D. Ribotta[1,2,3], Marcela L. Martinez[2,3,4]*

[1] Instituto de Ciencia y Tecnología de los Alimentos Córdoba (ICYTAC - CONICET) Universidad Nacional de Córdoba, Córdoba, Argentina.

[2] Instituto de Ciencia y Tecnología de los Alimentos (ICTA), Facultad de Ciencias Exactas, Físicas y Naturales, Universidad Nacional de Córdoba, Córdoba, Argentina.

[3] Departamento de Química Industrial y Aplicada, Facultad de Ciencias Exactas, Físicas y Naturales, Universidad Nacional de Córdoba, Córdoba, Argentina.

[4] Instituto Multidisciplinario de Biología Vegetal (IMBIV, CONICET), Universidad Nacional de Córdoba, Argentina

[5] Unidad de Investigación y Desarrollo en Tecnología Farmacéutica (UNITEFA, CONICET), Universidad Nacional de Córdoba, Argentina.

[6] Instituto de Investigación y Desarrollo en Ingeniería de Procesos y Química Aplicada (IPQA, CONICET), Universidad Nacional de Córdoba, Argentina.

[7]School of Pharmacy, Queen's University Belfast, Medical Biology Centre, 97 Lisburn Road, Belfast, BT9 7BL, Northern Ireland, UK.

*Corresponding author. IMBIV, CONICET, Universidad Nacional de Córdoba, Av. Vélez Sársfield 1611, 5000 Córdoba, Argentina; e-mail address: marcelamartinez78@hotmail.com, marcela.martinez@unc.edu.ar.

E-mail addresses: gabrielabordon90@gmail.com, maria.gabriela.bordon@mi.unc.edu.ar (M.G. Bordón), a.paredes@qub.ac.uk (A.J. Paredes), nahuelc03@gmail.com (N.M. Camacho), cpenci@gmail.com (María Cecilia Penci), agustingonzalez24@gmail.com (A. González), sdpalma@fcq.unc.edu.ar (S.D. Palma), pribotta@agro.unc.edu.ar (P.D. Ribotta).

Abstract

In this research, complex coacervation between soy protein isolate (SPI) and gum arabic (GA) constituted a preliminary step for developing chia oil (CO)-in-water emulsions suitable for subsequent spray drying. The contributions of total biopolymer concentration, SPI-GA ratio w/w and ionic strength on coacervate yield (CY) were quantified through a 3x6x4 factorial design. The SPI-GA ratios that gave the highest CY values (1-1 and 2-1) were selected to prepare emulsions and blank dispersions (devoid of CO). The preparation process included four well-defined sequential steps: high speed homogenization, high pressure homogenization, complex coacervation and a carrier addition (maltodextrin). The emulsification step, the SPI-GA ratio and the presence of CO had a significant effect ($p \leq 0.05$) on ζ-Potential, apparent viscosity, structural recovery of the systems, gel strength and cross-linking. The microencapsulation process preserved the quality of CO (2.18±0.01 h), as reflected by enhanced oxidative stability indices (around three times higher than bulk CO, 5.65-6.84 h) and non-significant changes in α-Linolenic acid after spray drying and *in-vitro* digestion processes (60-66.53% relative abundance). In addition, thermogravimetric analysis (TGA) and Fourier transform infrared spectroscopy (FTIR) helped corroborate the stability of CO within the powders' structure. Finally, different characteristics of powders were significantly influenced ($p \leq 0.05$) by the presence of CO, especially the color, flowability and sorption-dependent properties: the monolayer content (W_m) and the bulk moisture diffusivity.

Keywords: chia oil; complex coacervation; spray drying; rheological properties; dynamic vapor sorption; microstructure.

Abbreviations

a* CIE-LAB coordinate (redness-greenness)

a_W water activity (-)

A stiffness parameter of the Friedrich and Heymann model ($Pa.rad^{-\alpha}.s^{\alpha}$)

AO available oil after *in-vitro* digestion (%, g/100 g oil incorporated in the formulation)

b* CIE-LAB coordinate (yellowness-blueness)

C parameter of the GAB equation

CC complex coacervation

CI Carr's Index (%)

CO chia oil

CY coacervate yield (%, dry basis)

D_{eff} bulk moisture diffusion coefficient (m^2/s)

D [3,2] Sauter mean diameter (μm)

D [4,3] de Brouckere mean diameter (μm)

DVS dynamic vapor sorption

EE encapsulation efficiency (%, dry basis)

FTIR Fourier transform infrared spectroscopy

G' storage modulus (Pa)

G" loss modulus (Pa)

GA gum arabic

HA hysteresis area (Pa/s)

HPH high pressure homogenization

HR Hausner ratio (-)

HSH high speed homogenization

K consistency index ($Pa.s^n$)

K_g parameter of the GAB equation

L* CIE-LAB coordinate (lightness)

MD DE 5 maltodextrin (Dextrose equivalence = 5)

MOC moisture content (%, wet basis)

n flow index (-)

OSI oxidative stability index (h)

RH relative humidity (%)

PDI polydispersity index (-)

SSA specific surface area (μm^{-1})

SEM scanning electron microscopy

SOC surface oil content (%, dry basis)

SPI soy protein isolate

T_g glass transition temperature (°C)

TGA thermogravimetric analysis

TO total oil content of microcapsules (%, dry basis)

T_{onset} onset temperature for decomposition phenomena (°C)

W_{eq} equilibrium moisture content (g/100 g dry solids)

W_I initial moisture content (g/100 g dry solids)

W_m monolayer moisture content or monolayer capacity (g/100 g dry solids)

$WG_{0.8}$ weight gain during moisture sorption at $a_W = 0.8$

WI whiteness index (-)

WL weight loss (%, wet basis)

YI yellowness index (-)

Greek symbols

α order of relaxation function (-)

$\dot{\gamma}$ shear rate (s^{-1})

η dynamic viscosity (Pa.s)

η_{100} dynamic viscosity at 100 s^{-1} (Pa.s)

η^* complex viscosity (Pa.s)

ρ_A aerated density ($kg.m^{-3}$)

ρ_T tapped density ($kg.m^{-3}$)

τ shear stress (Pa)

Φ volume fraction of the dispersed phase (-)

ω frequency (s^{-1})

1. Introduction

The consumption of omega-3 fatty acids is associated with well known health benefits: prevention of cancer, cardiovascular and inflammatory diseases [1]. Chia (*Salvia hispanica* L.) oil (CO) is the major vegetable source of α-Linolenic acid (ALA, C18:3), thus fortified food and nutritional supplements development with chia has been extensively encouraged [2]. However, CO is highly susceptible to oxidation due to the unsaturated structure of omega-3 fatty acids [3], which ultimately decreases the nutritional value of foods and negatively impacts their sensory properties [2-5]. Hence, the need for omega-3 rich oils protection through microencapsulation technologies is justified [4,5].

Among microencapsulation methods, complex coacervation constitutes a unique alternative for lipids due to the high encapsulation efficiency achieved and the mild processing conditions [6]. It is an associative phase separation phenomenon induced by modifications of the pH, temperature, ionic strength or solubility of the dissolving medium [7]. In complex coacervation, a protein and a polysaccharide exert strong attractive interactions between each other, mostly of electrostatic nature. Biopolymer complexes aggregate forming a three-dimensional network due to charge neutralization. In order to minimize the interfacial free energy of the system, the mixture phase separates on a macroscopic level: one phase being rich in the two biopolymers (the coacervate phase) and the other phase being rich in the solvent [7].

Complex coacervation can be used to produce food emulsions and gels; nonetheless, for some food applications, drying is an essential unit operation to obtain the coacervated microcapsules in powder form. These microcapsules can be recovered from the reaction mixture by several techniques: filtration, dehydration with alcohol or silica, oven drying, vacuum drying, freeze drying or spray drying [6]. The latter two have been reported as the two most commonly employed technologies. However, spray drying is probably the most attractive for the food industry due to its simple and continuous operation mode, the existence of several types of equipment, and the relatively low production costs [2,3,6]. Generally, nearly spherical particles of 5- 50 µm size are obtained by spray drying, whereas freeze drying yields a dried lump that must be ground to a powder by mechanical disintegration, increasing the possibility of premature core release due to the capsule's break down [3,6]. Consequently, spray drying is explored in the present work to prepare dry chia oil microcapsules after complex coacervation.

During the last ten years, soy proteins have become one of the most utilized plant origin-emulsifiers, probably owing to the extensive production of this legume worldwide [8]. Nonetheless, it has been informed that the emulsions formulated with these proteins alone are not very stable [8]. Therefore, complex coacervation between soy proteins (SP) and anionic polysaccharides has been studied to enhance the stability of emulsions. In the present work, gum arabic (GA) was selected as the partner for soy protein isolate (SPI) in order to encapsulate CO by complex coacervation

and subsequent spray drying, mainly because of its dual role as both emulsifier and drying matrix [9].

So far, complex coacervation between SP and GA has been described by Jun-Xia et al. [10] and Dong et al. [11,12] in terms of isothermal titration calorimetry, turbidity, sedimentation and ternary phase boundaries. The influence of different variables on coacervate yield (CY) was analyzed. However, the majority of the previous studies on SPI+GA complex coacervation were made in a narrow range of total biopolymer concentration values (0-1%); moreover, these low values of total solid content affect the process yield and the energy required to evaporate the solvent in the drying operations that produce the final microparticles [6]. The study of Dong et al. [11] is an exception, given that the authors explored the formation of SPI+GA complex coacervates in a wider spectrum of total concentration values (0-10%) w/w. Therefore, the first objective of this research (**Fig. 1**) was to analyze the effect of three experimental factors (total biopolymer concentration, SPI-GA ratio and ionic strength) on CY variability by means of a factorial design, including a wide range of total solid content (0.8 – 16%) w/v. This was carried out to formulate an emulsion suitable for subsequent spray drying.

Different materials have been encapsulated in SPI+GA complex coacervates: sweet orange oil [10], fish oil [13], flaxseed oil [12], soybean oil [14], and anthocyanins [15]. The properties of oil-in-water emulsions prepared by different routes, and of the powders obtained by spray [10] or freeze drying [13,15] were analyzed. In this regard, the second objective (**Fig. 1**) of this research contributed to understand systematically how important properties of parent blank dispersions and/or spray-dried powders based on SPI+GA complex coacervates are affected by the incorporation of the core material (CO). Special discussion is devoted to some properties, which to the best of the authors' knowledge, have been reported scarcely (or have not been addressed) for delivery systems developed from SPI+GA complex coacervates as wall materials. First, the thixotropic behavior and viscoelastic properties of blank dispersions and chia oil-in-water emulsions through process steps: high speed homogenization (HSH), high pressure homogenization (HPH), complex coacervation (CC) and maltodextrin addition (MD DE 5). In this regard, Kong et al. [14] evaluated the rheological properties of soybean oil-in-water emulsions prepared with SPI+GA coacervates, but there is no mention of the assessment of time-dependent behavior. Dong & Cui [16] studied the viscoelastic properties of SPI+GA coacervates. Nonetheless, the analysis was carried out only with a low solid content (1%), away from the concentration of interest for drying applications, and was not performed for oil-in-water emulsions. Second, the chemical stability of the core within the microcapsules' structure was evaluated by the oxidative stability index (Rancimat test) and the fatty acid profile of the encapsulated oil before and after *in-vitro* digestion. Third, specific properties were evaluated on blank microparticles (devoid of chia oil) and microcapsules: the moisture sorption behavior, the bulk moisture diffusion coefficient, the glass transition temperature, the thermal stability assessed by thermogravimetric analysis (TGA) and the Fourier transformed infrared (FTIR) spectra.

2. Materials and Methods

2.1. Materials.

Chia oil (CO) was extracted from seeds coming from Salta province (Nutracéutica Sturla SRL, Argentina), according to Martínez et al. [17] in a pilot-plant screw press (Komet Model CA 59 G, IBG Monforts, Germany). Soy protein isolate (SPI) SUPRO E with 90% protein on fat free, dry-weight basis was purchased from The Solae Company (Argentina); gum Arabic (GA) (Alland & Robert, France) and maltodextrin (MD) DE 5 (Lorelite 5, Companhia Lorenz, Brazil) were purchased from a local distributor (Distribuidora NICCO, Argentina). Petroleum ether (Biopack, Argentina), analytical grade citric acid, sodium hydroxide and sodium chloride (Cicarelli Laboratories, Argentina) were purchased from a local distributor (Proveduría Científica, Argentina). Alpha-amylase, pepsin and pancreatin were purchased from Sigma Aldrich (St. Louis, MO, USA). Other reagents used were analytical or HPLC grade (Cicarelli, Argentina).

2.2. Preparation of wall material dispersions.

SPI was dispersed in Milli-Q water at room temperature for 1 h, with stirring [3]; GA was dispersed in hot Milli-Q water (50 °C) according to Di Battista et al. [18]. Stock SPI (10% w/v) and GA (30% w/v) suspensions were prepared and subsequently diluted in order to obtain the desired total biopolymer (SPI+GA) concentrations (% w/v) and SPI-GA ratios (w/w). The corresponding levels for the total biopolymer concentration and the SPI-GA ratio are given in section 2.3. Finally, SPI and GA suspensions were kept overnight at 4 °C for complete hydration [3].

2.3. Biopolymers' (SPI+GA) complex coacervates.

Biopolymers' (SPI+GA) complex coacervates were prepared according to the methodology described by Jun-Xia et al. [10] with brief modifications, which can be found explained in detail in section A1.1 (supplementary material).

Preliminary analysis for the identification of the pH (pH_{opt}) that maximizes the coacervate yield (CY) at each SPI-GA ratio were carried out at a concentration of 0.8% w/v: ζ-Potential, turbidity and CY determinations as function of pH.

The CY was determined according to the methodology proposed by Dong et al. [11], after allowing the systems to reach the equilibrium for 2 days, with subsequent centrifugation (10100*g,* 20 min, 15 °C) to separate the coacervate phase and oven drying at 105 °C. CY (%, dry basis) was estimated as (m_f/m_0) x 100 (**Eq. A1**, supplementary material), being m_f and m_0 the mass of dry coacervates and the initial mass of both SPI+GA, respectively.

Once the pH_{opt} was identified, a replicated 3x6x4 randomized factorial design (144 runs) was performed in order to evaluate the effect of three factors on CY. The corresponding levels for each factor were: SPI-GA ratio (1-2, 1-1, 2-1) w/w, total biopolymer concentration (0.8, 1, 4, 8, 12, 16%)

w/v, ionic strength (0, 0.1, 0.5, 1 M NaCl). Moreover, the pH_{opt} values determined in the preliminary analysis (supplementary material) were: 3.00, 3.15 and 2.75 for 1-1, 2-1 and 1-2 SPI-GA ratios, respectively.

The complete methodology and results for the preliminary analysis and the factorial design are given in the supplementary material. The contributions to CY variability due to the experimental factors and their interactions were studied by Multifactorial ANOVA techniques (**Table A1**). Moreover, optical and confocal fluorescence microscopy images of the coacervates are included.

2.4. Parent emulsions and blank dispersions.

The reasons for developing protein-polysaccharide coacervates as stabilizers are their surface activity, their ability to increase the viscosity of the dispersions and to form gel-like thick adsorbed layers [19].

The conditions for maximum CY (supplementary material) must be adapted in order to obtain chia seed oil-in-water emulsions suitable for spray drying. Given that CY increases at low concentration of the wall-forming materials, the solid content is usually low, affecting the drying process [6]. However, the microencapsulation efficiency may be improved and the energy that must be supplied to evaporate the solvent may be reduced by increasing the solid content of the emulsions [9]. A trade-off must be reached between a high solid content to enhance the thermal efficiency of drying [20], but not too high to suppress CY and difficult the pumping of the feed. In order to reach a high solid content in the feed, the 12% w/v total concentration for the SPI+GA suspension was selected, in spite of the fact that CY values were not the highest: the corresponding mean for the values observed was 41%, lower than those recorded between 0.8-8% w/v (**Figs.A3 A-C**). On the other hand, the 16% w/v total concentration was not selected because of two reasons. First, not all the systems containing a 16% w/v total solids (especially those with a non-zero ionic strength) evidenced a macroscopic phase separation after 2 days of stabilization, according to the methodology of Dong et al. [11] for CY determination. Second, because of the viscosity increase in SPI suspensions prepared with such a solid content, which might hinder the transport of emulsions. Liu et al. [21] reported a rise in the consistency index from 5.28 to 221.11 $Pa.s^n$ at 25 °C, when the solids' concentration of suspensions containing only SPI increased from 16 to 22%.

According to multiple-variable analysis, there were statistically significant differences ($p \leq 0.05$) for CY values. The means were in the following order for SPI-GA ratios: 1-2 (29.88%)< 1-1 (41.14%)< 2-1 (55.26%), evidencing a clear tendency depicted in **Figs.A3 A-C** for all the total concentrations and in **Fig.A4**. Therefore, the 1-2 SPI-GA ratio was omitted because of the poor CY. In addition, CY values for 0 M NaCl were the highest (with a mean of 49.78%) among the ionic strength levels (**Fig.A5**).

Finally, blank dispersions devoid of chia oil and parent emulsions with a 12% w/v total concentration (SPI+GA), 1-1 SPI-GA and 2-1 SPI-GA ratios (w/w), and 0 M NaCl were prepared and characterized.

2.4.1. Preparation.

Chia oil-in-water emulsions were prepared according to Bordón et al. [22,23]. SPI and GA dispersions were mixed by high speed homogenization (HSH) (16000 rpm, 5 min, Ultraturrax IKA T18, Janke & Kunkel GmbH, Staufen, Germany). Thereafter, CO was incorporated drop-wise into the SPI+GA suspensions, in a 2-1 w/w wall-core ratio ([SPI+GA]/CO) by HSH (16000 rpm, 2 min). These coarse emulsions were homogenized at 700 bar and 1 cycle by high pressure homogenization (HPH) (laboratory-valve homogenizer, EmulsiFlex C5, Avestin, Ottawa, ON, Canada). The pH of fine emulsions was adjusted to pH_{opt} (3.0 and 3.15 for 1-1 and 2-1 SPI-GA ratio, respectively) with 3 M citric acid to induce complex coacervation (CC) between SPI and GA, and the reaction was completed with stirring (40 °C, 30 min). Maltodextrin (MD DE 5) (4% w/v in final emulsions) was incorporated with stirring before spray drying. The total solid content of emulsions corresponding to wall materials was 16% w/v; the oil content was 6% w/v. Finally, parent blank dispersions devoid of CO were prepared following the same procedure.

2.4.2. Characterization.

2.4.2.1. Size distribution of droplets in parent emulsions.

The size distribution of droplets through the preparation steps described in 2.4.1 was determined by laser diffraction according to Julio et al. [24] and with a LA 950V2 Horiba analyzer (Kyoto, Japan). The *volume*-weighted de Broucker (D[4,3]) and the *surface*-weighted Sauter (D[3,2]) mean diameters, and the polydispersity index (PDI) [24] were calculated. The relative refractive index used (refractive index of oil/refractive index of water) was 1.10 [2]. The measurements were conducted at 25 °C.

The specific surface area of droplets (SSA) was calculated according to Di Giorgio et al. [25]:

$$SSA = \frac{6\Phi}{D[3,2]} \qquad (1)$$

where Φ is the volume fraction of the dispersed phase.

2.4.2.2. ζ-Potential.

The emulsions and blank dispersions were diluted using Milli-Q water to yield a concentration of 0.8% w/v total solids for ζ-Potential measurements [26], as performed for the complex coacervates' characterization (Supplementary text A1.2). The measurements were carried out at 25 °C (Nano Zetasizer, Malvern Instruments, Worcestershire, UK) and equilibration time was 120 s.

2.4.2.3. Rheological properties.

The rheological properties of emulsions and blank dispersions after each preparation step were evaluated using a controlled-stress rheometer, Physica MCR 301 Anton Paar (Physica Messtechnik, Germany). A plate-cone geometry (1°, 50 mm diameter) was used, working with a 0.05 mm-gap as described by González et al. [27]. The measurements were carried out at 25 °C.

2.4.2.3.1. Time-dependent steady shear properties.

A logarithmic increasing shear rate with a continuous ramp from 1 to 100 s^{-1} in 3 min was applied. The constant shear rate was then maintained for 1 min and afterward, the speed decreased logarithmically for 3 min until it stopped. The Power law rheological model was fitted to the experimental ascending curves (shear stress, τ versus shear rate,$\dot{\gamma}$).

$$\tau = K\dot{\gamma}^{n} \quad (2)$$

where, *K* is the consistency index ($Pa.s^n$) and *n* is the flow index.

The structural relaxation of the systems was given by the area (HA) within the hysteresis loop (Pa/s), which was calculated with the Rheoplus/32 V3.10 software (Anton Paar).

2.4.2.3.2. Viscoelastic properties.

Frequency sweeps (0.1-100 Hz) were performed to assess the network structure at 1% strain, being 10% strain the upper limit for the linear viscoelastic range (LVR) previously determined from amplitude sweeps. Storage (G') and loss (G'') moduli, and complex viscosity (η*) as a function of frequency were analyzed.

The Friedrich & Heymann mechanical model [28] was used to evaluate the network extension and strength. According to this model, η* could be expressed as:

$$\eta^* = A\,\omega^{(\alpha-1)} \quad \text{with } 0 < \alpha < 1 \quad (3)$$

where, A is the elastic strength of the material ($Pa.rad^{-\alpha}.s^{\alpha}$) and α is the order of relaxation function, which is used to identify the network extension [29].

2.5. Blank microparticles and chia oil microcapsules.

2.5.1. Spray drying process.

The spray drying process was performed as described by González et al. [3]. A laboratory-scale Mini Spray Dryer Büchi B-290 (Büchi Labortechnik AG, Flawil, Switzerland) with a two-fluid nozzle (0.7 mm-cap orifice diameter) was used. The process conditions were: dying-air inlet temperature: 130±1 °C; air outlet temperature: 80±1 °C; atomization-air flow rate: 1050 L/h; pump setting (feed volumetric flow rate): 10% (2.8 mL/min); aspirator setting (drying-air volumetric flow rate): 100% (38 m^3/h).

2.5.2. Characterization of chia oil microcapsules.

2.5.2.1. Size distribution of droplets in reconstituted emulsions.

Microcapsules (10 g) were dispersed in distilled water up to 100 mL of final emulsion at 25 °C and vortexed 3 times for 2 min. Thereafter, measurements were performed as described in 2.4.2.1, and D[4,3] and D[3,2] diameters, the PDI and SSA were calculated.

2.5.2.2. Encapsulation efficiency.

The encapsulation efficiency (EE) was calculated from the ratio of total oil in microcapsules (TO) and the surface oil content (SOC):

EE=[(TO-SOC)/TO] x 100 (4)

where total and surface oil contents were determined according to González et al. [3]. In the present research, no significant differences ($p>0.05$) were observed between the initial amount of chia oil added to the formulation and the total oil content of microcapsules determined by Soxhlet extraction [3], which was 26.63±0.89 % (dry basis).

SOC was informed as g oil/100 g dry solids (%, dry basis).

2.5.2.3. In-vitro *digestion and fatty acid composition.*

Digestive fluids that simulated the three stages of digestion were prepared for *in vitro* experiments to investigate the amount of chia oil available for intestinal absorption. Simulated salivary (SSF), gastric (SGF) and intestinal (SIF) fluids were prepared according to Timilsena et al. [30] and González et al. [4]. Afterward, 4 g of microcapsules were exposed to 12.5 mL of SSF (2 min, 37 °C) in an orbital shaker. The pH was adjusted to 2.0 with 1 M HCl and 25 mL of SGF were added. Samples were exposed to SGF during 2 h at 37 °C. Finally, the pH of the mixture was adjusted to 7.0 with 1 M NaOH, and 25 mL of SIF were added and mixed for 2 h at 37 °C [22].

The lipid compounds were extracted from the mixture with *n*-hexane (3 x 50 mL), the solvent was completely evaporated, and the mass of remaining oil ($m_{oil,2}$) was weighed and compared to the initial mass of oil ($m_{oil,1}$) added during the preparation of microcapsules. The available oil after *in-vitro* digestion (*AO*) was calculated as ($AO = (m_{oil,2}/m_{oil,1}) \times 100$) [4].

Finally, the fatty acid composition of bulk and microencapsulated CO, before and after *in-vitro* digestion, was analyzed by gas chromatography (Perkin-Elmer, Shelton, CT, USA) according to Martínez et al. [31].

2.5.2.5. Oxidative stability index.

Microencapsulated and bulk CO were subjected to accelerated oxidation in a Rancimat apparatus (743 Rancimat METROHM, Herisau, Switzerland). The conditions were: 100 ºC, air flow rate: 20 $L.h^{-1}$, 1.00±0.50 g of sample [3].

2.5.3. Characterization of blank microparticles and chia oil microcapsules.

2.5.3.1. Moisture content.

Moisture content analysis for each sample was performed with a moisture analyzer operated with infrared heating (model MB45 OHAUS, USA) [3].

2.5.3.2. Water activity.

The a_w of the powders was measured using an Aqua-Lab Water Activity Meter (208 Series 3, Decagon Devices Inc., USA) at 25.0±0.5ºC [32].

2.5.3.3. Sorption isotherms.

The sorption equilibrium moisture content of microparticles was determined by a gravimetric method using a Dynamic Vapor Sorption (DVS) instrument (Advantage 1 Model, Surface Measurement Systems Ltd., UK) at 25 °C, according to Gili et al. [33]. The humidity inside a temperature-controlled chamber was regulated by varying a dry nitrogen flow through a humidification step. The mass changes were recorded with a microbalance inside the chamber. The powders were evenly distributed and lightly compressed in the DVS pan by tapping its bottom, on the laboratory bench surface, and forming a thin slab with an average thickness across the pan of 2.3 mm [34].

The theoretical model of Guggenheim, Anderson & de Boer (GAB) was fitted to the experimental data (Eq.5). It is based on the theory of multi-layer physical adsorption and has been widely used to describe the sorption behavior of different powders [34,35].

$$W_{eq} = \frac{W_m \mathrm{C} K_g a_W}{(1-K_g a_W)(1-K_g a_W+\mathrm{C} K_g a_W)} \quad (5)$$

where, W_{eq} is the equilibrium moisture content (kg H_2O.100 kg^{-1} dry solids), W_m is the monolayer content (kg H_2O.100 kg^{-1} dry solids) (also called monolayer capacity) [35], C and K_g are model constants and a_W is the water activity.

2.5.3.3.1. Estimation of the bulk moisture diffusion coefficient.

The sorption data were used to calculate the bulk moisture diffusion coefficient according to Maidannyk et al.[37], based on the assumption of moisture sorption limited by diffusion. This calculated value is an apparent (not a true) diffusion coefficient through the matrix [34]. The solution of the Fick's second law for one-dimensional slab is expressed as follows [34]:

$$\Gamma = \frac{(W-W_{eq})}{(W_I-W_{eq})} = \frac{8}{(\pi)^2} \sum_{\mathrm{n}=0}^{\infty} (2\mathrm{n}+1)^{-2} \exp \frac{\mathrm{Deff}(2\mathrm{n}+1)^2(\pi)^2 t}{4L^2} \quad (6)$$

where, W_{eq}, W_I and W are the equilibrium, the initial and the moisture content at time t, respectively; L is the thickness of the slab. Moreover, the above equation assumes uniform initial moisture content and constant surface moisture and density [37].

Eq. (6) was solved by the slope method [34]:

$$\mathrm{Deff} = -\left(\frac{4L^2}{\pi^2}\right) \mathrm{x\ Slope} \quad (7)$$

where the slope in Eq. 7 was determined from a plot of ln(Γ) versus time.

2.5.3.4. ζ-Potential.

Powders were redispersed using Milli-Q water to yield a concentration of 0.8% w/v total solids for

ζ-Potential measurements, as in 2.4.2.2.

2.5.3.5. Color.

A CM600d spectrophotometer (Konica-Minolta, Japan) with 8-mm measurement aperture, D65 illuminant and a 10°-angle was used for color determinations according to González et al. [4]. Color was recorded as CIE-LAB values, *L** (lightness), *a** (redness-greenness), *b** (yellowness-blueness). Whiteness (WI) and yellowness (YI) indexes were calculated according to Rodríguez et al. [38]:

$WI=L^* - 3b^*$ (8)

$YI=(142.86 \times b^*)/L^*$ (9)

2.5.3.6. Flowability.

Powder flowability was assessed using the Carr's Index (CI) and the Hausner Ratio (HR) [38]:

$CI=[(\rho_T - \rho_A)/\rho_A] \times 100$ (10)

$HR=(\rho_A / \rho_T)$ ~~$\times 100$~~ (11)

where ρ_A and ρ_T are the aerated and tapped bulk density, respectively:

$\rho_A=m_0/V_0$ (12)

$\rho_T=m_0/V_T$ (13)

where m_0, V_0 and V_T are the mass of solids, the volume directly read from the cylinder, and the constant volume reached after tapping softly ten times, respectively.

2.5.3.7. Glass transition temperature (T_g) and thermogravimetric analysis (TGA).

Glass transition temperature determinations and TGA were carried out in a DSC/TGA Discovery analyzer (TA Instruments, New Castle, DE, USA) following the methodologies by Bordón et al. [22,23].

2.5.3.8. Fourier transform infrared spectroscopy in Attenuated total reflectance mode (FTIR-ATR).

FTIR-ATR analysis (FTIR Nicolet 5-SXC spectrometer, Thermo Fisher Scientific, Waltham, MA, USA) were performed using a ZnSe crystal with a 45°-incidence angle. The spectra of samples were collected as an average of 32 scans recorded at 4 cm^{-1} resolution, using air as background [27].

2.5.3.9. Scanning electron microscopy (SEM).

The morphology of chia oil microcapsules and blank microparticles was assessed by scanning electron microscopy (SEM). Powders were adhered to a double-sided adhesive tape mounted on SEM stubs, coated with chrome under vacuum and examined with a scanning electron microscope (SEM, LSM5 Pascal; Zeiss Oberkochen, Germany) [3].

2.6. Statistical Analysis.

Analytical determinations in this study were the averages of triplicate measurements. The analysis of variance was performed with One-way ANOVA at the 95% level ($p \leq 0.05$) of significance. Whenever ANOVA indicated a significant difference, multiple-sample comparisons were run by Fisher's least significant difference (LSD) procedure ($p \leq 0.05$). In addition, the effects of the experimental factors, and of the interaction among them, on different variables were analyzed by Multifactorial ANOVA techniques ($p \leq 0.05$). Multiple-variable analysis was applied to establish correlations (Pearson test) between different pairs of variables. Data analysis was carried out with the Statgraphics Centurion XVI.I software (Statpoint Technologies, USA).

3. Results and Discussion.

3.1. Blank dispersions and parent emulsions.

3.1.1. *Size distribution of droplets in parent emulsions*

Many authors highlighted the influence of emulsion characteristics on the properties of powders, especially droplet size distribution [32]. These results are useful for tracking changes due to interaction between components, environmental conditions, processing transformations, prolonged storage or simulated gastric digestion [39].

Table 1 shows the contribution of the process steps and SPI-GA ratio on the size distribution-related parameters of emulsions. In addition, the complete distribution after each step is depicted in **Figs.2 A** (1-1 SPI-GA ratio) and **B** (2-1 SPI-GA ratio). D[4,3] and D[3,2] mean diameters are given in **Figs.2 C** (1-1 SPI-GA ratio) and **D** (2-1 SPI-GA ratio). The SSA and the PDI are shown in **Figs.2 E** (1-1 SPI-GA ratio) and **F** (2-1 SPI-GA ratio). As can be seen from **Table 1**, both factors and their interaction exert a significant ($p \leq 0.05$) effect on D[4,3], D[3,2], PDI and SSA.

Coarse emulsions (HSH) showed a bimodal distribution (**Figs.2 A**, **B**), with the following D[4,3] and D[3,2] (**Figs.2 C**, **D**): 28.13±2.09 µm and 12.87±1.55 µm (1-1 SPI-GA ratio) and 34.52±0.20 µm and 12.87±1.44 µm (2-1 SPI-GA ratio), respectively. The statistically significant differences ($p \leq 0.05$) between D[4,3] and D[3,2] at each step are indicated with bold capital letters in **Figs.2 C**, **D**. The greater the difference between both diameters, the more heterogeneous the size distribution [25]. PDI and SSA (**Figs.2 E**, **F**) were: 8.41±0.58 and 0.034±0.004 μm^{-1} (1-1 SPI-GA ratio) and 6.73±0.58 and 0.029±0.003 μm^{-1} (2-1 SPI-GA ratio), respectively. For both ratios, significant changes ($p \leq 0.05$) could be observed after high HPH, compared with coarse emulsions. First, the distribution shifted from bimodal to unimodal. Second, D[4,3], D[3,2] diameters, and PDI were significantly reduced ($p \leq 0.05$): 11.45±0.02 µm, 3.74±0.00 µm and 0.18±0.00 (1-1 SPI-GA ratio), and 11.26±0.00 µm, 1.30±0.10 µm and 0.52±0.01 (2-1 SPI-GA ratio), respectively. The difference between D[4,3] and D[3,2] decreased for both ratios, compared with HSH. In turn, SSA was significantly increased ($p \leq 0.05$) as a result of more mechanical work applied to the system: 0.112±0.000 μm^{-1} (1-1 SPI-GA ratio) and 0.292±0.030 μm^{-1} (2-1 SPI-GA ratio). As an emulsion passes through the valve of the homogenizer, it is subjected to a combination of shear, cavitation

forces and turbulent flow conditions, which disrupt the large droplets into smaller ones [40].

The formation of complex coacervates (CC) led to an increase in the droplet size, compared with HPH. For the 1-1 SPI-GA ratio, this increase was neither significant ($p>0.05$) in the D[4,3] diameter (13.08±0.00 μm) nor in the PDI (0.29±0.00). Nonetheless, significant ($p\leq0.05$) changes were noticed in the D[3,2] diameter (12.81±0.09 μm) and in the SSA (0.029±0.000 μm^{-1}), which are related to the exposed surface area of the droplets. These latter changes may be explained by the deposition of the coacervate, which binds together several oil droplets and encapsulates them within the same microcapsule. This phenomenon yields polynucleated entities. Therefore, the coacervate layer around the droplets significantly increases their D[3,2] diameter and decreases their SSA [41]. For the 2-1 SPI-GA ratio, significant changes ($p\leq0.05$) were observed in D[4,3] (14.58±0.31 μm), D[3,2] mean diameters (8.79±0.05 μm) and in the SSA (0.043±0.000 μm^{-1}). Once more, the PDI was not significantly ($p>0.05$) affected (0.35±0.02).

The final step is the addition of MD DE 5, which may cause depletion flocculation in emulsions, as explained by Gharsallaoui et al. [42]. Nonetheless, in this study, no significant ($p>0.05$) changes were evidenced in the size distribution-related parameters (**Figs.2 A**, **C** and **E**), compared with the previous step (CC).

3.1.2. *ζ-Potential measurements in blank dispersions and emulsions.*

The charge on the particle surface dictates its interactions with other charged species [24]. Moreover, the effective charge accumulated on the surface determines the dispersion or aggregation of particles [43]. ζ-Potential was tracked through the preparation steps in blank dispersions and parent emulsions. **Figs.3 A** and **B** show the changes for 1-1 SPI-GA and 2-1 SPI-GA ratios, respectively. In addition, the contributions of the process step, SPI-GA ratio, presence of the core (incorporation of chia oil) and their interactions on the ζ-Potential variability are shown in **Table 2**. According to this table, all the individual and interaction effects were statistically significant ($p\leq0.05$), except for the interaction SPI-GA ratio x incorporation of the core material.

Multiple-variable analysis showed significant ($p\leq0.05$) differences between the 2-1 and the 1-1 ratios. Indeed, higher absolute values of ζ-Potential were observed for the former ratio, especially at HSH and HPH stages. Above pH_{opt}, i.e. before CC, SPI and GA are negatively charged (**Fig.A1 A**). As there are more negative charges available from SPI per GA chain with the 2-1 ratio [11], higher absolute values of ζ-Potential were recorded.

An outstanding tendency that both ratios share, with and without CO, is the significant rise ($p\leq0.05$) in the absolute value of ζ-Potential after HPH, compared with HSH. Song et al. [43] also observed a rise in the ζ-Potential of SPI dispersions (from around 16 to 30 mV) while increasing the number of passes through a high pressure homogenizer. According to the authors, the disruption of the molecules increases their specific surface area, accumulating more charges on the surface. In the present study, although the increase in ζ-Potential was less pronounced than the observed by Song et al. [43], it seems to be in line with the explanation given by the authors.

As can be seen from **Figs. 3 A** and **B**, once the electrical neutralization in the systems is reached (the CC step), no significant differences ($p>0.05$) in ζ-Potential were recorded, regardless of the incorporation of chia oil. The charges of SPI and GA were neutralized, as expected after complex coacervation [44]. No more charges were added with the incorporation of MD DE 5, as reflected by no significant changes ($p>0.05$) in ζ-Potential. This was also observed by Julio et al. [24], who reported a non-significant effect of maltodextrin on ζ-Potential values of chia oil-in-water emulsions. Electrostatic repulsion is one of the main mechanisms for the stabilization of emulsions owing to the charges adsorbed at the O/W interface [24]. Nonetheless, the stability of SPI+GA complex-coated oil droplets may not be due to electrostatic repulsions, given the observed ζ-Potential values at complex coacervation conditions: -1.33±0.05 mV (2-1 SPI-GA ratio) and -0.38±0.02 mV (1-1 SPI-GA ratio). Gharsallaoui et al. [42] made similar observations for pea protein isolate-pectin complex-stabilized emulsions. At pH=2.4, the absolute value for ζ-Potential was around 2.8 mV, which was not sufficient to provide stabilization. The authors postulated a plausible mechanism, which may also account for the stability of emulsions at complex coacervation in our work. The thickness of the interfacial membranes would provide steric repulsion between droplets. Indeed, small oil droplets (mean diameter<50 μm) could be encapsulated by complex coacervates more easily than large droplets, forming a homogeneous thick film at the surface of droplets [41].

3.1.3. *Rheological properties.*

The time-dependent steady shear and viscoelastic properties of blank dispersions and emulsions were evaluated. As performed with properties in sections 3.1.1 and 3.1.2, the contributions of the process step, SPI-GA ratio, presence of CO and their interactions were assessed by Multifactorial ANOVA techniques. The results are given in **Table 3**.

3.1.3.1. *Time-dependent steady shear properties.*

Figs.A8 A-D (supplementary material section) show the shear stress vs. shear rate curves for blank dispersions and emulsions through the preparation steps. The Power law parameters (K, n) for the ascending curves, the corresponding determination coefficient (R^2), the apparent viscosity at 100 s^{-1} (η_{100}) and the hysteresis loop area (HA), are given in **Table 4**.

As can be noticed from the figures and table, the systems exhibited a shear-thinning behavior ($n<1$) and the Power law model was successfully fitted to the rheological data ($R^2>0.90$). This was mainly attributed to the inclusion of SPI in the formulations ($n=0.321$-0.336, **Fig.A7 A**), given that GA and MD DE 5 suspensions were Newtonian ($n>0.950$) within the range of shear rates (**Fig.A7 B**). These observations were in accordance with Di Battista et al. [18] for GA, Siemons et al. [45] for MD DE 5, and with Liu et al.[21] for SPI. In addition, another feature shared by the systems as a consequence of the presence of SPI was the non-zero HA (**Fig.A7 A**), indicating a time-dependent shear-thinning behavior [21].

The process steps, the interactions with the SPI-GA ratio and the presence of the core had

significant influence ($p \leq 0.05$) on K, n, η_{100} and HA (**Table 3**). The first outstanding characteristic is the increase in K, η_{100} and HA (**Table 4**) from HSH to HPH in blank dispersions and emulsions. After HPH, the SSA of droplets increases and the repulsive interactions become more significant above the pH of complexation. Hence, the viscosity of the system is risen and less structural recovery is observed (HA increases) [46]. This would explain the highest K, η_{100} and HA values recorded for HPH.

Upon CC, the ζ-Potential of the complexes is close to neutral. Particle-particle over particle-solvent interactions are favored, thereby releasing water to the bulk of the suspensions [19]. K and η_{100} are significantly ($p \leq 0.05$) reduced due to the release of water. Moreover, given the increased attractions between SPI and GA, the structural recovery of the systems upon shear is enhanced and HA decreased ($p \leq 0.05$).

The addition of MD has a key role in the formulations and during drying. Recently, it has been demonstrated that low DE-maltodextrins (mainly DE 5) yield droplets with an elastic skin after the locking point, thereby withstanding surface compression more efficiently than higher DE-maltodextrins (≥21) [45]. In the present study, maltodextrin addition led to an increase in the apparent viscosity η_{100}. Moreover, K increased significantly ($p \leq 0.05$) from complex coacervation to maltodextrin addition only for the parent emulsion formulated with the 2-1 SPI-GA ratio (**Table 4**). The most important benefit was the significant ($p \leq 0.05$) reduction in HA, which may be attributed to the junction zones formed by lower DE-maltodextrins [47]. This would improve the structural recovery of the systems by increasing the attractive interactions among their components.

Multiple-variable analysis showed significant ($p \leq 0.05$) increases in K, η_{100} and HA with a higher protein content. However, no significant influence ($p > 0.05$) was noticed on the flow index, n (**Table 3**). The increases may be explained by more entanglement among protein molecules at higher concentrations, causing more intermolecular friction [21].

The rheological behavior of parent emulsions through the preparation steps was similar to that exhibited by blank dispersions, given that the viscosity of emulsions is directly proportional to that of the continuous phase [46]. Nonetheless, the presence of the CO yielded significant rises in K, η_{100} and HA, and a reduction in n compared with blank dispersions ($p \leq 0.05$). The addition of oil droplets disturbs the flow of the fluid, promoting greater energy dissipation [39].

3.1.3.2. *Viscoelastic properties.*

The mechanical spectra of blank dispersions and emulsions through the preparation steps are depicted in **Figs.A10 A-D** (supplementary material section). The Friedrich & Heymann model parameters (A, α) and the determination coefficients (R^2) are given in **Table 5**.

The presence of CO, SPI-GA ratio and their interactions had significant ($p \leq 0.05$) influence on the viscoelastic properties. Regarding the steps, only the interaction with the presence of CO was significant ($p \leq 0.05$) (**Table 3**). Special features were noticed. First, the complex viscosity (η^*) in the systems decreased almost linearly with frequency, evidencing a shear-thinning behavior (data not

shown). Second, gel-like structures were suggested, given the dominance of the storage modulus (G') over the loss modulus (G''). This may be attributed to the presence of SPI [27], because GA and MD DE 5 were Newtonian and structureless [46]. No cross-over points were observed (**Figs.A10 A-D**) within the frequency range, except for two systems with 1-1 SPI-GA ratio at high frequencies: the blank dispersion after HSH and the parent emulsion upon CC (**Figs.A10 A**, **C**). The mechanical spectra of SPI suspensions evidenced a cross-over by the end of the frequency range when less protein was present, i.e., the 1-1 SPI-GA ratio (**Fig. A9**), suggesting that a high oscillatory shear may weaken the original gel structure [48]. These latter observations may account for the cross-over points noticed in two systems with the 1-1 SPI-GA ratio.

The Friedrich & Heymann model [28] successfully adjusted the η* data (R^2>0.98) (**Table 5**). The network strength was determined by the material stiffness parameter (A). A significant (p≤0.05) increase was noticed in the systems from HSH to HPH, possibly attributed to the thickening of the layer between droplets and of the aqueous continuous phase [45], that also affected properties like K, η_{100} and HA. Indeed, the highest A values were recorded after HPH, and particularly for emulsions, the increase in A was accompanied by a decrease in the droplet diameter [50]. After CC and MD DE 5 addition the net repulsion forces were reduced, and the viscosity of the systems was decreased due to the release of water. Therefore, the gel strength was reduced compared with the HPH stage [29], which was reflected by lower A values (p≤0.05).

The order of relaxation function (α) is an exponent indicative of the nature of cross-linking and varies between 1 for viscoelastic liquids at low frequency and 0 for solid materials [16]. The lower this value, the higher the number of interactions [51]. Moreover, these cross-links between macromolecules are in a dynamic equilibrium between formation and rupture, and contribute to the preservation of the structures during the observation times [49]. Values between 0.014-0.203 were noticed, evidencing the elastic behavior typically observed in gel-like systems [49].

A higher protein content significantly (p≤0.05) affected the A parameter. Indeed, the gel strength was increased due to the thicker continuous phase [49]. Finally, regarding the incorporation of CO, significant differences (p≤0.05) in the means of α among blank dispersions (0.144) and parent emulsions (0.082) were evidenced by multiple-variable analysis. The physical interactions between the core and the wall materials [44], besides those existing previously among biopolymers in the continuous phase, may involve a higher number of interactions in emulsions compared with blank dispersions and α was reduced. Indeed, when a protein and certain polysaccharides with a minor protein fraction such as gum arabic [9] are present, they are physically-adsorbed at the oil/water interface by hydrophobic interactions [39,46].

3.2. Blank microparticles and chia oil microcapsules.

3.2.1. *Characterization of chia oil microcapsules.*

The main properties studied for chia oil microcapsules are shown in **Table 6**. In addition, statistically significant differences (p≤0.05) observed for the properties between both SPI-GA ratios

are indicated with lower-case letters. The size distributions (**Fig.A11**), D[4,3] and D[3,2] diameters, the PDI and SSA of oil droplets in reconstituted emulsions were analyzed in the same manner as done with parent emulsions (section 3.1.1) because they provide valuable information about the stability of oil droplets during atomization [32]. The properties (D[4,3], D[3,2], SSA and PDI) for parent emulsions fed to the dryer are given between parenthesis in **Table 6**. Significant ($p \leq 0.05$) differences were observed between both SPI-GA ratios, and between parent and reconstituted emulsions. Upon atomization, D[4,3] and D[3,2] diameters, PDI and SSA changed significantly for the 1-1 ratio. On the other hand, a significant ($p \leq 0.05$) increment was observed only in the D[4,3] diameter for the 2-1 ratio, (**Fig.A11** and **Table 6**). Fission and re-coalescence of droplets occur during atomization [9], and the predominance of this phenomenon may explain the increase in D[4,3]. In turn, the higher viscosity of the feed for the 2-1 compared with the 1-1 ratio (**Table 4**) might have offered more resistance to disintegration [9].

Surface oil content (SOC) and encapsulation efficiency (EE) of powders were studied. As can be seen from Table 6, no statistically significant ($p > 0.05$) differences were observed between the SOC and EE means of both SPI-GA ratios. Low SOC values (<5%, d.b.) and EE>80% were recorded. Ixtaina et al. [2] and Us-Medina et al. [32] reported similar EE for microencapsulated chia oil.

Regarding the available oil after in-vitro digestion, it has been discussed by many authors that non-lipid components in delivery systems (proteins, polysaccharides and fibers) affect the rate of lipid digestion [30]~~[30]~~. In a first step, the oil available to be absorbed after ingestion and passage through the gastrointestinal tract was determined. Second, the fatty acid composition after digestion was analyzed. The results showed that a high amount of the oil originally contained in powders was released (**Table 6**). The difference between 2-1 and the 1-1 ratios was not statistically significant ($p > 0.05$). Also, the values were similar to those reported for chia oil microcapsules using only SPI as wall material, which were obtained by freeze-drying [4] and supercritical CO_2-assisted impregnation [52]; 94.83±2.57% and 95.69±4.28% of the available oil was released in the former and latter studies, respectively. Timilsena et al. [30] informed a high release (>95%) for chia oil encapsulated in a different complex coacervate system, composed of chia mucilage and chia protein isolate.

The fatty acid composition for microencapsulated oils before and after the *in-vitro* digestion is depicted in **Fig. A12**. Regarding the α-Linolenic acid content, a slight but not significant reduction ($p > 0.05$) was found for samples (around 60%) compared with bulk oil (66.53±0.01%), supporting the chemical stability of the core through the emulsification, drying and *in-vitro* digestion stages. Once more, this was in agreement with González et al. [4] and Gañán et al. [52].

It was observed that the induction times were significantly ($p \leq 0.05$) higher for microencapsulated oils than for bulk oil (2.18±0.01 h). The protection factor, defined as the quotient between the induction times for microencapsulated and bulk oil, was 3.01±0.19 and 2.69±0.07 for 1-1 and 2-1 SPI-GA ratios, respectively. A significantly ($p \leq 0.05$) lower protective effect was noticed for the latter ratio. Similarly, Di Giorgio et al. [25] informed a lower oxidative stability of fish oil as the protein

content of the wall increased, despite the higher encapsulation efficiency. The authors offered an explanation, which may account for the observations in our research. It has been suggested that the presence of proteins facilitates an immediate formation of an elastic membrane at the surface of droplets during drying [20]. Therefore, the higher the protein content, the faster the shift of the drying kinetics to the falling rate period. In turn, the increased resistance to evaporation during this period might rise the particle temperature, promoting the generation of more oxidation compounds [25].

3.2.2. *Characterization of chia oil microcapsules and blank microparticles.*

Table 7 summarizes the contributions of SPI-GA ratio, the presence of CO and their interaction on the variability of some properties analyzed on chia oil microcapsules and blank microparticles. Moreover, the results for these properties and the statistically significant differences ($p \leq 0.05$) observed are given in **Table 8**.

3.2.2.1. *Moisture content and water activity.*

Moisture content (MOC) and a_w (25 °C) of powders were 3.25–3.93% (w.b.) and 0.297–0.404, respectively, in agreement with recommended values for food powders [53]. As can be seen from **Table 8**, both properties were significantly ($p \leq 0.05$) influenced by SPI-GA ratio, the presence of CO and the interactions between them. MOC and a_w values were significantly ($p \leq 0.05$) higher for blank microparticles and these results may be explained in terms of the moisture sorption behavior.

3.2.2.2. *Sorption isotherms.*

The sorption experimental data at 25 °C for are shown in **Figs.4 A**, **B**. High determination coefficients ($R^2 > 0.98$) were obtained for the fitting of the sorption data of powders. As regards the goodness of fit of the GAB equation, it has been demonstrated that a realistic description of sigmoidal-type isotherms is achieved when the K_g and C parameters are kept within the regions: $0.24 < K_g \leq 1$ and $5.67 \leq C \leq \infty$ [54]. As can be observed from **Table 8**, K_g and C parameters fell within the specified ranges.

A significantly ($p \leq 0.05$) higher W_m was observed for blank microparticles, compared with those for chia oil microcapsules, evidencing more available sorption sites for the former products. The W_m values may indicate that the presence of an oily core reduces the water-holding capacity of powders [55]. Moreover, these values may explain the significantly ($p \leq 0.05$) higher amount of water adsorbed by blank microparticles at 25 °C and a_W = 0.8, i.e., $WG_{0.8}$ (**Table 8**). In turn, the $WG_{0.8}$ values followed the same tendencies as those of MOC and a_w (25 °C) (section 3.2.2.1) and may be related to them. All powders exhibited a high moisture sorption capacity, as judged by the $WG_{0.8}$ values recorded (≥15%) w/w [56].

Higher values of W_m (6.315 kg water/100 kg dry solids) for microencapsulated chia oil were

reported by Escalona-García et al. [36], who used a whey protein concentrate-mesquite gum blend as wall material. These authors also observed much higher C values (35.229±1.059) than those of this study, indicating a stronger interaction between water and the primary sorption sites (**Table 8**). Notwithstanding, many authors suggested that the C parameter may not have any physical meaning, and may be a result of a mathematical compensation between parameters during the curve fitting [36]. As regards K_g, the values were not significantly ($p>0.05$) different among powders (**Tables 7** and **8**) and were close to 1, indicating that the multilayer molecules showed bulk liquid-like properties.

3.2.2.2.1. *Bulk moisture diffusion coefficient.*

The bulk moisture diffusion coefficient during sorption was estimated from the DVS data by the slope method [34,37]. Once more, it should be reminded that the calculated values are apparent (not true) diffusion coefficients through the matrix. The results as function of relative humidity (% RH) are shown in **Fig.4 C** and were based on sorption kinetics limited by diffusion, constant diffusion coefficient for each %RH (this could change from one stage to another) and homogeneous particle size [37,55]. Coefficients of the same order of magnitude were reported by Murrieta-Pazos et al. [55] in skim and whole milk powders. According to **Fig.4 C**, the highest values were recorded for blank microparticles, in accordance with the W_m and $WG_{0.8}$ values. Once more, these observations support the fact that the presence of CO affects the water-uptake capacity of the biopolymer matrix. Bell-like curves were obtained, in agreement with Murrieta-Pazos et al. [55] and Maidannyk et al. [37]. The authors attributed the bell shape of the curves to a series of phenomena that may also account for the observations in this research. First, adsorption occurs rapidly due to the presence of materials with a high moisture sorption capacity [55]. Nonetheless, the plasticizing effect of water becomes predominant at a certain %RH. Next to the maximum, the caking and impermeabilization of the macroscopic structure may take place, which in turn may entail changes in the particle porosity [57]. Therefore, the sorption rates decrease [55].

3.2.2.3. *Color.*

The color of powders is of paramount importance because it determines the macroscopic aspect of the products in which they are incorporated as ingredients [3]. Whitish powders are preferred over others with a yellowish appearance, given that a yellow color can be due to spoilage reactions [38]. As can be seen in **Table 8**, significant ($p\leq0.05$) increases were noticed in the a* and b* parameters, as well as in YI due to the incorporation of the core. In addition, WI decreased significantly ($p\leq0.05$), while no changes were found in L*. Gañán et al. [52] reported a similar effect on the color of soy protein microparticles after the supercritical CO_2-assisted impregnation of CO, as expected from the original color of the oil.

3.2.2.4. *Flow properties.*

Approximately 75% of the chemical manufacturing processes involve the handling of particulate solids at some stage [58] and a problem associated with microencapsulated oils is their poor flowability [57]. This flow is governed by physical properties, for instance, particle size distribution and shape, moisture content and time-consolidation [38]. Moreover, differing trends have been reported for the roles of the adsorbed moisture and the non-encapsulated oil on the cohesive forces that arise between particles [57,58]. Electrostatic forces between particles may also affect the flow properties [53], although other factors might explain the differences observed in the present study.

The flowability of powders was assessed through the Carr's Index (CI) and the Hausner ratio (HR). According to **Table 8**, blank microparticles exhibited a better flowability than chia oil microcapsules. First, CI values for the former products are below the limit of a free-flowing powder (~ 25%), whereas values between 26–31% indicate a poor flow [38]. The higher compressibility noticed in microcapsules evidences a more cohesive powder [57]. The same trend was observed in HR values, from which easy (HR<1.25) and difficult-to-fluidize (HR>1.40) powders were distinguished [38]. Similarly, Quispe-Condori et al. [59] informed better flowing properties (HR<1.25 and CI<25%) for the wall material powder (zein) than for flax oil microcapsules (HR>1.42 and CI>29%). However, no plausible reasons for these results were given.

In this research, both types of powders exhibited a similar particle size and shape, according to the SEM images given in **Fig. 5** (section 3.2.2.1). Hence, these latter two properties might not explain completely the flowing properties observed. Second, the electrostatic forces may not account greatly for the differences observed between blank microparticles and microcapsules, because no significant ($p>0.05$) changes in ζ-Potential were noticed (**Table 8**). Third, it has been generally accepted that the powders' moisture content may be considered as inversely correlated to their capacity to flow [60]. In this regard, it is interesting to point out that the moisture content values for blank microparticles (**Table 8**) were significantly higher ($p\leq0.05$) than those of the microcapsules, however, they exhibited better flowing properties. Therefore, these observations would indicate that the difference in moisture contents would not help provide a complete explanation. Fourth, authors like Drusch et al. (2006) explained that the non-encapsulated oil fraction is a limiting factor concerning flowability, which might turn the microcapsules' surface more hydrophobic [61] and hamper the flow because of a more cohesive powder [57]. Hence, this latter factor should be considered and might explain the results observed in the present study.

3.2.2.5. *Glass transition temperature and thermogravimetric analysis (TGA).*

The importance of T_g lies on maintaining the powders' quality, because the storage of these products at temperatures above T_g may cause crystallization phenomena and an enhanced oxygen diffusivity, compared with a glassy matrix [32]. The glass transition temperature (T_g) was neither influenced ($p>0.05$) by the SPI-GA ratio nor by the presence of the core, as shown in **Tables 7** and **8**. Moreover, the DSC curves, including CO, are depicted in **Figs.A13 A**, **B**. The

region of the inflection point in the curves is delimited within circles. The values recorded for T_g were in accordance with those reported for anhydrous MD DE 5 [9], GA [62], and SPI [63].

The thermogravimetric performance of CO, wall materials, blank microparticles and chia oil microcapsules was assessed (**Figs.A14 A-H**). The onset temperatures (T_{onset}) at which the highest weight loss starts are indicated with arrows. It was found that all powders showed two main stages of mass loss within the temperature range studied. The first stage (<100 °C) may be related to the desorption of water [43], and had a small weight loss for all powders. The onset temperatures for the second degradation stage (T_{onset}) in powders were in agreement with values reported for our wall materials, and may be attributed to the decomposition of long molecular amine units of SPI (~270 °C) [43,44], and to the thermal degradation profile of polysaccharides [64]. As can be seen in **Tables 7** and **8**, no significant ($p>0.05$) differences were observed between SPI-GA ratios and between microcapsules and blank microparticles for T_{onset} and weight loss (WL) values.

As regards CO, the weight loss observed up to 350 °C is associated with the first stage of vegetable oils' thermal decomposition, where the unsaturated fatty acids' decomposition starts [65]. The T_{onset} for bulk CO was 210±2 °C, reflecting a gain in thermal stability by the microencapsulated oils because of their significantly ($p\leq0.05$) higher T_{onset}.

3.2.2.6. *Fourier transform infrared spectroscopy (FTIR).*

FTIR analysis was performed in wall materials (**Fig.A15**), CO, blank microparticles and microcapsules (**Figs.A16 A**, **B**). Analysis of the oil showed from 2800 to 3000 cm^{-1} absorption bands related to the C-H bonds: asymmetric (CH_2 at 2934 cm^{-1}) and symmetric stretching (CH_2 at 2854 cm^{-1}) [65]. The fingerprint region below 1600 cm^{-1} shows a more intricate profile of identified absorption bands: 1459 (-C-H_2-), 1238 (-CH_3), 914 (-C-O-, ester), 864 (=CH_2) and 720 cm^{-1} (fatty acids with *cis* double bonds) [66]. According to Lavanya et al. [66], an intense absorption at 1150 cm^{-1} evidenced the presence of α-Linolenic acid in chia oil. In our research, this band (1149 cm^{-1}) was identified in bulk and microencapsulated chia oils, but not in blank microparticles (arrows in **Figs.A16 A**, **B**). This characteristic band was attenuated in the microcapsule, indicating the location of the oil within the matrix [65]. Other bands identified in powders were located at 3000-3500 cm^{-1} (O–H stretching), 2926 (C–H stretching), 1735-1750 (ester, C=O stretching), 1617 (amide I, C=O stretching), 1365 (O-H bending), and 1075 (C-O stretching), in accordance with Bordón et al. [23]. It is worth pointing out special features observed after coacervation. First, the bands identified at 1544 (amide II, N–H bending) and at 1225 (amide III, C–N stretching) in SPI (**Fig.A15**) and at 1612 cm^{-1} (C=O stretching, free carboxyl groups) in GA, in agreement with Huang et al. [67] and Nayak et al. [68], respectively, were shifted towards lower wave numbers in blank microparticles and in microcapsules. This might indicate interactions between functional groups [27,67]. Second, all the spectra showed a broad band at around 3000-3600 cm^{-1}, evidencing an enhanced hydrogen bonding compared with that of SPI alone. This was also noticed by Huang et al. [67] upon soy protein isolate-chitosan complex coacervation.

The formation of new bands was not observed for microcapsules, meaning that no new chemical bonds between the core and the wall materials were established and the predominance of physical interactions between them [44].

3.2.2.7. *Scanning electron microscopy (SEM).*

SEM micrographs of microcapsules and blank microparticles are shown in **Fig. 5**. Surface analysis revealed that non-spherical particles with continuous and homogeneous surfaces were obtained. The droplets undergoing a high evaporation rate in a co-current system may expand and give such kind of particles [20]. Both microcapsules and blank microparticles presented shriveled and concave surfaces, which are typically produced by spray drying processes [9], and with no apparent pores or fractures. Some individual particles (especially in the case of blank microparticles, **Figs. 5 C**,**D**,**G** and **H**), or tiny agglomerates (especially in the case of microcapsules, **Figs. 5 A**,**B**,**E** and **F**) as a result of the fine particles produced by two-fluid nozzle atomizers, could be observed [20].

4. Conclusions.

The complex coacervation process between soy protein isolate (SPI) and gum arabic (GA) was explored as a preliminary step for the development of chia oil-in-water emulsions suitable for spray drying. Besides emulsions, blank dispersions (devoid of CO) were prepared in order to analyze the influence of the core material on ζ-Potential, the time-dependent steady shear and viscoelastic properties before spray drying. The contributions of the process step, the SPI-GA ratio and their interactions were also assessed. The first outstanding result extracted from this research is the importance of maltodextrin addition (MD DE 5) to enhance the structural recovery of emulsions and blank dispersions during shear, besides its well-known role as a carrier agent during drying.

An exhaustive characterization was performed on chia oil microcapsules and blank microparticles. The changes in some properties of powders such as color, flowability and the sorption behavior after the incorporation of chia oil were expected. Indeed, the monolayer content or capacity of the GAB model and the bulk moisture diffusion coefficients showed differing trends depending on the incorporation (or not) of CO. Moreover, the differences between blank microparticles and chia oil microcapsules could be objectively quantified by this study.

It is worth highlighting the accurate protection of the core provided by the microencapsulation process, as evidenced by the enhanced protection factors compared with bulk chia oil. If a different oil had been encapsulated, the first outstanding difference that would have been expected is, precisely, the oxidative stability. Indeed, each oil has its own fatty acid composition and minor compounds (free fatty acids, mono and diacylglycerols, phospholipids, chlorophylls, thermally oxidized compounds, carotenoids, tocopherols, among others), which exert a great influence on its oxidative stability.

The oxidative stability of microencapsulated oils represents an important physico-chemical

property that should be preserved when up-scaling. In this regard, the spray drying experiments performed at laboratory scale help define the critical process parameters and the target physico-chemical properties of powders, which should then be considered during the scale-up. Hence, it is important to point out two aspects. First, that many important process variables and properties of products (especially those regarding flowability) may change compared with the laboratory scale. These differences are mainly attributed to the initial droplet size, tower designs, residence times, among other factors, which are known to vary across scales. Second, if these results were potentially used by the food industry, any up-scale approach should try to preserve the chemical quality of oils and a co-current spray-air contact, like in the present study, which is ideal for heat-sensitive materials.

The α-Linolenic acid content was not significantly ($p>0.05$) reduced after the spray drying and *in-vitro* digestion processes. Other outstanding conclusions were the observation of a higher onset temperature for thermal decomposition in microcapsules than in bulk chia oil (TGA), and the identification of an absorption band at 1149 cm^{-1}, which indicated the presence of α-Linolenic acid in bulk and encapsulated oils (FTIR-ATR). This latter analysis also helped confirm the predominance of physical interactions between the core and the encapsulating wall.

Supplementary research is needed in different areas. First, “clean label” ingredients should be explored as potential substitutes for maltodextrin. For instance, fiber-based carriers, inulin and pectins from different origin have been described as successful alternatives by several recent review articles. Second, to study the drying mechanisms and influence of spray drying operating conditions on the properties of powders. A more detailed knowledge of spray drying and improved predictions of process variables and properties of powders (outlet temperature and relative humidity of drying air, particle size and moisture content of powders, among others) may be achieved through mathematical models of diverse complexity. Finally, to design scale-up experiments, which are currently being performed by our research group. Indeed, chamber deposits could be minimized because of the high investments in new spray dryer capacities, which usually involve improved performances to produce better-quality powders.

Acknowledgements.

This research was financed with grants from CONICET, SeCyT-UNC and FONCyT (BID PICT 2014-2283) from Argentina. The authors would also like to acknowledge the Iberoamerican Project CYTED 119RT0567, and Laboratorio de Análisis Térmico (LAT) from FCQ-UNC for the thermal behavior analysis.

The authors declare no conflict of interest.

References.

[1]S.Punia, K.S. Sandhu, A.K. Siroha, S.B. Dhull, Omega 3-metabolism, absorption, bioavailability and health benefits–A review, PharmaNutrition 10 (2019) 1-7.

[2]V.Y.Ixtaina, L.M.Julio, J.R.Wagner, S.M.Nolasco, M.C.Tomás, Physicochemical characterization and stability of chia oil microencapsulated with sodium caseinate and lactose by spray-drying, Powder Technol. 271 (2015) 26-34.

[3]A.González, M.L.Martínez, A.J.Paredes, A.E.León, P.D.Ribotta, Study of the preparation process and variation of wall components in chia (*Salvia hispanica* L.) oil microencapsulation, Powder Technol. 301 (2016) 868-875.

[4]A.González, M.Martínez, A.E.León, P.D.Ribotta, Effects on bread and oil quality after functionalization with microencapsulated chia oil. J.Sci. Food Agric. 98 (13) (2018) 4903-4910.

[5]A.González, M.G.Bordón, M.C.Bustos, K.L.Córdova Salazar, P.D. Ribotta, M.L.Martínez, Study of the incorporation of native and microencapsulated chia seed oil on pasta properties, Int. J. Food Sci. Technol. (2020) https://doi.org/10.1111/ijfs.14623

[6]M. Mishra, Handbook of encapsulation and controlled release, CRC Press, Taylor & Francis Group, U.S., 2016.

[7]S.L.Turgeon, M.Beaulieu, C.Schmitt, C.Sanchez, Protein-polysaccharide interactions: phase-ordering kinetics, thermodynamic and structural aspects, Curr. Opin. Colloid Interface Sci. 8 (2003) 401-414.

[8]C.Burgos-Díaz, T.Wandersleben, A.M.Marqués, M.Rubilar, Multilayer emulsions stabilized by vegetable proteins and polysaccharides, Curr. Opin. Colloid Interface Sci. 25 (2016) 51-57.

[9]C.Anandharamakrishnan, S.Ishwarya, Spray drying techniques for food ingredient encapsulation, IFT Press, Wiley Blackwell, John Wiley & Sons, Ltd., UK, 2015.

[10]X.Jun-Xia, Y.Hai-Yan, Y.Jian, Microencapsulation of sweet orange oil by complex coacervation with soybean protein isolate/ gum arabic, Food Chem. 125 (2011) 1267-1272.

[11]D.Dong, Y.Hua, Y.Chen, X.Kong, C.Zhang, Q.Wang, Charge compensation, phase diagram, and protein aggregation in soy protein- gum arabic complex formation, J. Agric. Food Chem. 61 (2013) 3934-3940.

[12]D.Dong, Z.Qi, Y.Hua, Y.Chen, X.Kong, C.Zhang, Microencapsulation of flaxseed oil by soya proteins- gum arabic complex coacervation, Int. J. Food Sci. Technol. 50 (2015) 1785-1791.

[13]L.Costa de Conto, C.R.Ferreira Grosso, L.A.Guaraldo Gonçalves, Chemometry as applied to the production of omega-3 microcapsules by complex coacervation with soy protein isolate and gum arabic, LWT-Food Sci. Technol. 53 (2013) 218-224.

[14]X.Kong, C.Jia, C.Zhang, Y.Hua, Y.Chen, Characteristics of soy protein isolate/gum arabic-stabilized oil-in-water emulsions: influence of different preparation routes and pH, RSC Adv. 7 (2017) 31875-31885.

[15]M.Mansour, M.Salah, X.Xu, Effect of microencapsulation using soy protein isolate and gum

arabic as wall material on red raspberry anthocyanin stability, characterization, and simulated gastrointestinal coniditions, Ultrason. Sonochem. (2020) https://doi.org/10.1016/j.ultsonch.2019.104927

[16]D.Dong, B. Cui, Comparison of rheological properties of different protein/gum arabic complex coacervates, J. Food Process Eng. (2019) e13196. https://doi.org/10.1111/jfpe.13196

[17]M.L.Martínez, M.A.Marín, C.M.Salgado Faller, J.Revol, M.C.Penci, P.D.Ribotta, Chia (*Salvia hispanica* L.) oil extraction: study of processing parameters, LWT- Food Sci. Technol. 47 (2012) 78-82.

[18]C.A.Di Battista, D.Costenla, V.Ramírez-Rigo, J.Piña, The use of gum arabic, maltodextrin and surfactants in the microencapsulation of phytosterols by spray drying, Powder Technol. 286 (2015) 193-201.

[19]J.M.Rodríguez-Patino, A.M.R.Pilosof, Protein-polysaccharide interactions at fluid interfaces, Food Hydrocoll. 25 (2011) 1925-1937.

[20]K.Masters, Spray drying handbook (third ed.), Halsted Press, John Wiley & Sons Inc., U.S, 1979.

[21]P.Liu, H.Xu, Y.Zhao, Y.Yang, Rheological properties of soy protein isolate solution for fibers and films, Food Hydrocoll. 64 (2017) 149-156.

[22]M.G.Bordón, N.P.X.Alasino, N.Camacho, V. Yohaha, M.V.Defaín Tesoriero, P.D.Ribotta, M.L.Martínez, Spray-air contact and operating conditions in tall and short-type spray dryers affect relevant physico-chemical properties of microencapsulated chia oil (*Salvia hispanica* L.), Food and Bioprod. Process. (2021) In press doi: 10.1016/j.fbp.2021.03.008

[23]M.G.Bordón, N.P.X.Alasino, V.Martínez, R.Gauna Peter, R.Iturralde, P.D.Ribotta, M.L.Martínez, Influence of the spray drying operating conditions on the estimated drying kinetics of emulsion single droplets and the properties of microencapsulated chia oil, Powder Technol. 383 (2021) 302-317.

[24]L.M.Julio, C.N.Copado, B.V.K.Diehl, V.Y. Ixtaina, M.C. Tomás, Chia bilayer emulsions with modified sunflower lecithins and chitosan as delivery systems of omega-3 fatty acids, LWT-Food Sci. Technol. 89, (2018) 581-590.

[25]L.Di Giorgio, P.R.Salgado, A.M.Mauri, Encapsulation of fish oil in soybean protein particles by emulsification and spray drying, Food Hydrocoll. 87 (2019) 891-901.

[26]P.Kaushik, K.Dowling, C.J.Barrow, B.Adhikari, Complex coacervation between flaxseed protein isolate and flaxseed gum, Food Res. Int. 72 (2015) 91-97.

[27]A.González, G.Gastelú, G.N.Barrera, C.I.Álvarez Igarzabal, P.D.Ribotta, Preparation and characterization of soy protein films reinforced with celloluse nanofibers obtained from soybean by-products, Food Hydrocoll. 89 (2019) 758-764.

[28] C.Friedrich, L.Heymann, Extension of a model for crosslinking polymer at the gel point, J. Rheol. 32 (3) (1988) 235-241.

[29]E.Hasanvand, A.Rafe, Rheological and structural properties of rice bran protein-flaxseed

(*Linum usitissimum* L.) gum complex coacervates, Food Hydrocoll. 83 (2018) 296-307.

[30]Y. P.Timilsena, R.Adhikari, C.J.Barrow, B.Adhikari, Digestion behaviour of chia seed oil encapsulated in chia seed protein-gum complex coacervates, Food Hydrocoll. 66 (2017) 71-81.

[31]M.L.Martínez, M.G.Bordón, R.L.Lallana, P.D.Ribotta, D.M.Maestri, Optimization of sesame oil extraction by screw-pressing at low temperature, Food Bioprocess Technol. 10 (6) (2017) 1113-1121.

[32]U.Us-Medina, L.M.Julio, M.R.Segura-Campos, V.Y.Ixtaina, M.C.Tomás, Development and characterization of spray-dried chia oil microcapsules using by-products from chia as wall material, Powder Technol. 334 (2018) 1-8.

[33]R.D.Gili, M.Torrez Irigoyen, M.C.Penci, S.A.Giner, P.D.Ribotta, Physical characterization and fluidization design parameters of wheat germ, J. Food Eng. 212 (2017) 29-37.

[34]X.Yu, A.R.Schmidt, L.A.Bello-Perez, S.J.Schmidt, Determination of the bulk moisture diffusion coefficient for corn starch using an automated water sorption instrument, J. Agric. Food Chem. 56 (2008) 50-58.

[35]G.M. Kelly, J.A. O'Mahony, A.L. Kelly, D.J. O'Callaghan, Water sorption and diffusion properties of spray-dried dairy powders containing intact and hydrolysed whey protein, LWT-Food Sci. Technol. 68 (2016) 119-126.

[36]L.A.Escalona-García, R. Pedroza-Islas, R.Natividad, M.E.Rodríguez-Huezo, H.Carrillo-Navas, C.Pérez-Alonso, Oxidation kinetics and thermodynamic analysis of chia oil microencapsulated in a whey protein concentrate-polysaccharide matrix, J. Food Eng. 175 (2016) 93-103.

[37]V.Maidannyk, D.J.McSweeney, S.A.Hogan, S.Miao, S.Montgomery, M.A.E.Auty, N.A McCarthy, Water sorption and hydration in spray-dried milk protein powders: Selected physicochemical properties, Food Chem. 304 (2020) 125418. https://doi.org/10.1016/j.foodchem.2019.125418

[38]E.S.Rodríguez, L.M.Julio, C.Henning, B.W.K.Diehl, M.C.Tomás, V.Y. Ixtaina, Effect of natural antioxidant on the physicochemical properties and stability of freeze-dried microencapsulated chia seed oil, J. Sci. Food Agric. 99 (4) (2019) 1682-1690.

[39]D.J.McClements, Nanoparticle- and microparticle- based delivery systems. Encapsulation, protection and release of active compounds, CRC Press, Taylor & Francis Group, Boca Raton, FL, U.S., 2015.

[40]S.Schultz, G.Wagner, K.Urban, J.Ulrich, High-pressure homogenization as a process for emulsion formation, Chem. Eng. Technol. 27 (4) (2004) 361-368.

[41]D.Ach, S.Briançon, G.Broze, F.Puel, A.Rivoire, J-M.Galvan, Y.Chevalier, Formation of microcapsules by complex coacervation, Can. J.Chem. Eng. 93 (2) (2015) 183-192.

[42]A.Gharsallaoui, K.Yamauchi, O.Chambin, E.Cases, R. Saurel, Effect of high methoxyl pectin on pea protein in aqueous solution and at oil/water interface, Carbohydr. Polym. 80 (2010)

817-827.

[43]Song, C.Zhou, F.Fu, C. Zhilin, W. Qinling, Effect of high-pressure homogenization on particle size and film properties of soy protein isolate, Ind. Crop. Prod. 43 (2013) 538-544.

[44]L.Tavares, C.P.Zapata Noreña, Encapsulation of garlic acid extract using complex coacervation with whey protein isolate and chitosan as wall materials followed by spray drying, Food Hydrocoll. 89 (2019) 360-369.

[45]I.Siemons, R.G.A.Politiek, R.M.Boom, R.G.M.van der Sman, M.A.I.Schutyser, Dextrose equivalence of maltodextrins determines particle morphology development during single sessile droplet drying, Food Res. Int. 131 (2020) 108988. https://doi.org/10.1016/j.foodres.2020.108988

[46]D.J.McClements, Food Emulsions: Principles, Practice and Techniques, Ed. CRC Press, New York, U.S.,1999.

[47]I.S.Chronakis, On the molecular characteristics, compositional properties, and structural-functional mechanisms of maltodextrins: A review, Crit. Rev. Food Sci. Nutr. 38:7 (1998) 599-637.

[48]M.Anvari, D.Chung, Dynamic rheological and structural characterization of fish gelatin-gum arabic coacervate gels cross-linked by tannic acid, Food Hydrocoll. 60 (2016) 516-524.

[49]G.Lorenzo, G.Checmarev, N.Zaritzky, A.Calvane, Linear viscoelastic assessment of cold gel-like emulsions stabilized with bovine gelatin, LWT-Food Sci. Technol. 44 (2011) 457-464.

[50]S.Karaman, M.T.Yilmaz, M.Dogan, H.Yetim, A. Kayacier, Dynamic oscillatory shear properties of O/W model system meat emulsions: Linear viscoelastic analysis for effect of temperature and oil concentration on protein network formation, J. Food Eng. 107 (2011) 241-252.

[51]D.Gabriele, B.de Cindio, P.D'Antona, A weak gel model for foods, Rheol. Acta 40 (2) (2001) 120-127.

[52]N.Gañán, M.G.Bordón, P.D. Ribotta, A.González, Study of chia oil microencapsulation in soy protein microparticles using supercritical CO_2-assisted impregnation, J.CO_2 Util. 40 (2020) 101221. http://doi.org/10.1016/j.jcou.2020.101221

[53]B.R.Bhandari, B.P.Adhikari, Water activity in food processing and preservation, In: X.D. Chen, A.S. Mujumdar (eds.), Drying Technologies in Food Processing, John Wiley & Sons Ltd., West Sussex, UK, 2008, pp. 55-86.

[54]P. P.Lewicki, The applicability of the GAB model to food water sorption isotherms, Int. J. Food Sci. Technol. 32 (1997) 553-557.

[55]I.Murrieta-Pazos, C.Gaiani, L.Galet, B.Cuq., S.Desobry, J.Scher, Comparative study of particle structure evolution during water sorption: Skim and whole milk powders, Colloids Surf. B Biointerfaces 87 (2011) 1-10.

[56]Pharmacopeia, National formulatory (USP 24 NF 19), MD, U.S: Rockville, 2000.

[57]S.Drusch, Y.Serfert, K.Schwarz, Microencapsulation of fish oil with *n*-octenylsuccinate-derivatised starch: Flow properties and oxidative stability, Eur. J. Lipid Sci. Tech. 108 (2006)

501-512.

[58]E.Emery, J.Oliver, T.Pugsley, J.Sharma, J.Zhou, Flowability of moist pharmaceutical powders, Powder Technol. 189 (2009) 409-415.

[59]S.Quispe-Condori, M.D.A.Saldaña, F.Temelli, Microencapsulation of flax oil with zein using spray and freeze drying, LWT-Food Sci. Technol. 44 (2011) 1880-1887.

[60]E. Juarez-Enriquez, G.I. Olivas, P.B. Zamudio-Flores, E. Ortega-Rivas, S. Perez-Vega, D.R. Sepulveda, Effect of water content on the flowability of hygroscopic powders, J. Food Eng. 205 (2017) 12-17.

[61]A.H.Al-Muhtaseb, W.A.M.McMinn, T.R.A.Magee, Water sorption isotherms of starch powders. Part 1: mathematical description of experimental data, J. Food Eng. 61 (2004) 297-307.

[62]R.G.Barros Fernandes, S.Vilela Borges, D.Alvarenga Botrel, Gum arabic/starch/maltodextrin/inulin as wall materials on the microencapsulation of rosemary essential oil, Carbohydr. Polym. 101 (2014) 524-532.

[63]C-H.Tang, Z.Chen, L.Li, X-Q.Yang, Effects of transglutaminase treatment on the thermal properties of soy protein isolates, Food Res. Int. 39 (2006) 704-711.

[64]M.Castro-Cabado, F.J.Parra-Ruiz, A.L.Casado, J.San Román, Thermal cross-linking of maltodextrin and citric acid. Methodology to control the polycondensation reaction under processing conditions, Polym. Compos. 24 (6) (2016) 643-653.

[65]A.Guimarães-Inácio, C.R.Lopes Francisco, V.Maeda Rojas, R.de Souza Leone, P.Valderrama, E.Bona, et al., Evaluation of the oxidative stability of chia oil-loaded microparticles by thermal, spectroscopic and chemometric methods, LWT- Food Sci. Technol. 87 (2018) 498-506.

[66]M.N.Lavanya, T.Kathiravan, Moses J.A., C.Anandharamakrishnan, Influence of spray-drying conditions on microencapsulation of fish oil and chia oil, *Dry. Technol.* (2019) https://doi.org/10.1080/07373937.2018.1553181

[67]G-Q.Huang, Y-T.Sun, J.X.Xiao, J.Yang, Complex coacervation of soybean protein isolate and chitosan, Food Chem. 135 (2012) 534-539.

[68]A.K.Nayak, B.Das, R.Maji, Calcium alginate/gum arabic beads containing glibenclamide: Development and *in vitro* characterization, Int. J. Biol. Macromol. 51 (2012)1070-1078.

Figure Captions.

Figure 1. Scheme representing the organization of the whole manuscript.

Figure 2. Size distribution of droplets in parent emulsions through the preparation steps. Volume size distribution: (**A**) 1-1 SP-GA ratio w/w and (**B**) 2-1 SP-GA ratio w/w. D[4,3] and D[3,2] mean diameters: (**C**) 1-1 SP-GA ratio w/w and (**D**) 2-1 SP-GA ratio w/w. Specific surface area (SSA) and Polydispersity index (PDI): (**E**) 1-1 SP-GA ratio w/w and (**F**) 2-1 SP-GA ratio w/w. Process steps:

HSH: high speed homogenization, HPH: high pressure homogenization, CC: complex coacervation, MD DE 5: maltodextrin DE 5 addition. Significant differences (p≤0.05) for each variable are labeled with a unique color. Lower case letters indicate significant differences (p≤0.05) among steps. Bold capital letters in Figs. **C** and **D** show significant (p≤0.05) differences between D[4,3] and D[3,2] mean diameters at each step.

Figure 3. ζ-Potential in blank dispersions and parent emulsions through the preparation steps. (**A**) 1-1 SP-GA ratio w/w and (**B**) 2-1 SP-GA ratio w/w. The legend for parent emulsions includes "CO", which stands for chia oil incorporation. Process steps: HSH: high speed homogenization, HPH: high pressure homogenization, CC: complex coacervation, MD DE 5: maltodextrin DE 5 addition. Significant differences (p≤0.05) for blank dispersions or parent emulsions are labeled with a unique color. Lower case letters indicate significant (p≤0.05) differences among steps. Bold capital letters show significant differences (p≤0.05) between blank dispersions and parent emulsions at each step.

Figure 4. Sorption isotherms at 25 °C for chia oil microcapsules (MC) and blank microparticles (Blank MP). (**A**) 1-1 SP-GA ratio w/w and (**B**) 2-1 SP-GA ratio w/w. (**C**) Bulk diffusion coefficient.

Figure 5. SEM micrographs of chia oil microcapsules and blank microparticles. 1-1 SP-GA ratio w/w microcapsules: (**A**) 500 x, (**B**) 4000 x. 1-1 SP-GA ratio w/w blank microparticles: (**C**) 4000 x, (**D**) 11000 x. 2-1 SP-GA ratio w/w microcapsules: (**E**) 500 x, (**F**) 4000 x. 2-1 SP-GA ratio w/w blank microparticles: (**G**) 4000 x, (**H**) 11000 x.

Table 1. Multifactorial ANOVA of size distribution-related parameters in parent emulsions. **Significant p-values (≤0.05) are highlighted in bold.**

Factor	*p-value*			
	D [4,3]	D [3,2]	PDI	SSA
Process step (A)	**0.0000**	**0.0000**	**0.0000**	**0.0004**
SPI-GA ratio (B)	**0.0005**	**0.0003**	**0.0476**	**0.0000**
A x B	**0.0074**	**0.0125**	**0.0052**	**0.0002**

SPI-GA ratio (w/w); D [4,3], de Broucker mean diameter (μm); D [3,2], Sauter mean diameter (μm); PDI, polydispersity index; SSA, specific surface area (μm^{-1}).

Table 2. Multifactorial ANOVA of zeta potential (ζ- potential) in blank dispersions and parent emulsions.

Significant p-values (≤0.05) are highlighted in bold.

Factor	*p-value*
Process step (A)	**0.0000**
SPI-GA ratio (B)	**0.0002**
Core (C)	**0.0001**
A x B	**0.0021**
A x C	**0.0003**
B x C	0.1570

SPI-GA ratio (w/w), ζ- potential (mV). "Core (C)" corresponds to the incorporation of chia oil.

Table 3. Multifactorial ANOVA of rheological parameters in blank dispersions and parent emulsions. **Significant p-values (≤0.05) are highlighted in bold.**

Factor	*p-value*					
	K	n	η_{100}	HA	A	α
Process step (A)	**0.0000**	**0.0000**	**0.0000**	**0.0000**	**0.0000**	0.0523
SPI-GA ratio (B)	**0.0000**	0.4003	**0.0000**	**0.0000**	**0.0000**	**0.0236**
Core (C)	**0.0000**	**0.0007**	**0.0000**	**0.0000**	**0.0000**	**0.0000**
A x B	**0.0000**	**0.0001**	**0.0000**	**0.0014**	**0.0032**	0.8732
A x C	0.5572	**0.0003**	**0.0000**	**0.0003**	**0.0000**	**0.0003**
C x B	**0.0001**	**0.0035**	**0.0266**	**0.0000**	**0.0000**	**0.0007**

SPI-GA ratio (w/w); "Core (C)" corresponds to the incorporation of chia oil. K, consistency index ($Pa.s^n$); n, flow index; η_{100}, apparent viscosity at 100 s^{-1} (Pa.s); HA, hysteresis area (Pa/s); A, material stiffness parameter ($Pa.rad^{-\alpha}.s^{\alpha}$); α, order of relaxation function.

Table 4. Time-dependent steady shear properties of blank dispersions (BD) and parent emulsions (PE) through the preparation steps for different SPI-GA ratios.

		K		*n*		η_{100}		*HA*		R^2 (BD)	R^2 (PE)
		BD	**PE**	**BD**	**PE**	**BD**	**PE**	**BD**	**PE**		
SPI-GA 1-1	**HSH**	0.46^{aA}± 0.05	1.51^{aB}±0.05	0.40^{aB}± 0.04	0.23^{aA}± 0.02	0.03^{aA}± 0.00	0.05^{aB}± 0.00	100.76^{cA}±0.65	115.10^{cB}± 1.96	0.980	0.983
	HPH	1.41^{bA}± 0.13	4.26^{cB}±0.11	0.33^{aA}± 0.04	0.30^{bA}± 0.01	0.06^{bA}± 0.00	0.17^{dB}± 0.00	125.54^{dA}± 2.38	303.38^{dB}± 1.42	0.966	0.992
	CC	1.25^{bA}± 0.08	3.14^{bB}±0.08	0.33^{aA}± 0.02	0.31^{bA}± 0.01	0.06^{bA}± 0.00	0.14^{bB}± 0.00	92.65^{bA}±0.89	77.57^{bB}±0.05	0.987	0.991
	MD DE 5	1.16^{bA}± 0.16	3.17^{bB}±0.23	0.38^{aA}± 0.05	0.31^{bA}± 0.03	0.08^{cA}± 0.00	$0.1[illegible]^{cB}$± 0.00	24.61^{aA}±0.53	62.60^{aB}±1.42	0.968	0.978
SPI-GA 2-1	**HSH**	2.84^{bA}± 0.29	4.23^{cB}±0.11	0.34^{aA}± 0.09	0.26^{bA}± 0.01	$0.1[illegible]^{bA}$± 0.00	0.14^{bA}± 0.01	211.71^{cA}±3.80	553.70^{bB}± 1.28	0.946	0.991
	HPH	3.96^{cA}± 0.22	10.04^{dB}± 0.19	0.27^{bA}± 0.03	0.23^{bA}± 0.01	0.15^{cA}± 0.00	0.25^{cB}± 0.00	221.90^{cA}±13.24	693.09^{cB}± 0.86	0.973	0.992
	CC	1.90^{aA}± 0.03	2.04^{aA}±0.11	0.37^{aA}± 0.00	$0.4[illegible]^{aA}$± 0.02	0.11^{aA}± 0.00	0.13^{aA}± 0.00	138.58^{bA}± 6.17	163.28^{aB}± 6.96	0.997	0.996
	MD DE 5	1.90^{aA}± 0.22	3.14^{bB}±0.07	0.35^{aA}± 0.0[illegible]	0.37^{aA}± 0.02	0.12^{aA}± 0.00	0.19^{cB}± 0.00	89.71^{aA}±2.54	153.82^{aB}± 4.62	0.965	0.976

SPI-GA ratio (w/w); Process steps: HSH: High speed homogenization, HPH: High pressure homogenization, CC: Complex coacervation, MD DE 5: Maltodextrin DE 5 addition.

K, consistency index ($Pa.s^n$); n, flow index; η_{100}, apparent viscosity at 100 s^{-1} (Pa.s); HA, hysteresis area (Pa/s); R^2, determination coefficient for the Power law model.

Average values (n = 3) ± standard deviation are shown. For each SPI-GA ratio, lower case letters in columns indicate statistically significant differences (p≤0.05) among process steps; in each row, capital letters indicate significant differences (p≤0,05) between blank dispersions (BD) and parent emulsions (PE).

Table 5. Viscoelastic properties of blank dispersions (BD) and parent emulsions (PE) through the preparation steps for different SPI-GA ratios.

		A		*α*		R^2	
		BD	**PE**	**BD**	**PE**	**BD**	**PE**
SPI-GA 1-1	**HSH**	3.77^{cA}±0.01	6.72^{aB}±0.01	0.13^{aB}±0.00	0.14^{dA}±0.00	0.9996	0.9998
	HPH	6.82^{dA}±0.02	39.80^{cB}±0.02	0.15^{bB}±0.01	0.09^{cA}±0.01	0.9997	0.9997
	CC	2.42^{bA}±0.02	9.61^{bB}±0.02	0.20^{cB}±0.01	0.01^{aA}±0.00	0.9997	0.9998
	MD DE 5	1.55^{aA}±0.07	9.12^{bB}±0.02	0.20^{cB}±0.03	0.06^{bA}±0.01	0.9994	0.999
SPI-GA 2-1	**HSH**	20.89^{cA}±0.02	37.85^{cB}±0.02	0.14^{dB}±0.03	0.11^{dA}±0.01	0.9997	0.9997
	HPH	29.88^{dA}±0.01	73.77^{dB}±0.01	0.09^{aB}±0.00	0.10^{cA}±0.00	0.9999	0.9998
	CC	16.99^{bA}±0.01	23.18^{bB}±0.01	0.11^{bB}±0.00	0.06^{aA}±0.00	0.9999	0.9998
	MD DE 5	14.78^{aA}±0.01	20.30^{aB}±0.03	0.13^{cB}±0.01	0.08^{bA}±0.00	0.9999	0.9996

SPI-GA ratio (w/w); Process steps, HSH: High speed homogenization, HPH: High pressure homogenization, CC: Complex coacervation, MD DE 5: Maltodextrin DE 5 addition. A, material stiffness parameter ($Pa.rad^{-\alpha}.s^{\alpha}$); α, order of relaxation function; R^2, determination coefficient for the Friedrich & Heymann model. Average values (n = 3) ± standard deviation are shown. For each SPI-GA ratio, lower case letters in columns indicate statistically significant differences ($p \leq 0.05$) among process steps; in each row, capital letters indicate significant differences ($p \leq 0.05$) between blank dispersions (BD) and parent emulsions (PE).

Table 6. Physico-chemical properties of microcapsules.

	SPI-GA ratio	
Properties	**1-1**	**2-1**
D [4,3]	12.80[a]±0.09 (13.66±0.00)	19.60[b]±0.00 (16.85±0.26)
D [3,2]	9.03[a]±0.02 (12.85±0.02)	9.85[b]±0.09 (9.50±0.42)
SSA	0.042[b]±0.000 (0.029±0.000)	0.038[a]±0.000 (0.040±0.001)
PDI	0.21[a]±0.00 (0.57±0.01)	0.63[b]±0.01 (0.49±0.04)
SOC	4.58[a]±0.40	3.54[a]±0.47
EE	83.19[a]±1.48	87.02[a]±1.71
AO	93.69[a]±2.33	84.12[a]±7.03
OSI	6.84[a]±0.07	5.65[b]±0.08

SPI-GA ratio (w/w); the corresponding properties (D [4,3], D [3,2], SSA and PDI) for the parent emulsions fed to the dryer are given between parenthesis; D [4,3], de Broucker mean diameter (μm); D [3,2], Sauter mean diameter (μm); SSA, specific surface area (μm^{-1}); PDI, polidispersity index; SOC, surface oil content (%, d.b.); EE, encapsulation efficiency (%, d.b.);
AO, available oil after *in-vitro* digestion (%); OSI, oxidative stability index (h). Average values (n = 3) ± standard deviation are shown. Lower case letters in each row indicate statistically significant differences ($p \leq 0.05$) between SPI-GA ratios.

Table 7. Multifactorial ANOVA of different physico-chemical properties of powders. **Significant p-values (≤0.05) are highlighted in bold.**

		Factor		
		SPI-GA ratio (A)	Core (B)	AxB
p-value	*MOC*	**0.0001**	**0.0010**	**0.0010**
	$a_{W,25°C}$	**0.0000**	**0.0001**	**0.0000**
	$WG_{0.8}$	**0.0033**	**0.0000**	0.0643
	W_m	0.6172	**0.0001**	0.7941
	C	0.3881	0.5505	**0.0144**
	K_g	0.5806	0.6335	0.9107
	ζ-potential	**0.0142**	0.4714	0.2617
	L	**0.0493**	**0.0134**	0.3465
	a	0.8945	**0.0003**	0.2181
	b	**0.0180**	**0.0000**	0.2749
	WI	**0.0229**	**0.0001**	0.2868
	YI	**0.0196**	**0.0000**	0.2474
	CI	**0.0266**	**0.0002**	0.1367
	HR	0.0707	**0.0005**	0.4270
	T_g	0.3477	0.3977	0.6876
	T_{onset}	0.6396	0.1091	0.5122
	WL	0.5329	0.0663	0.9765

SPI-GA ratio (w/w); "Core (C)" corresponds to the incorporation of chia oil. MOC, moisture content (%, w.b.); $a_{W\ 25°C}$, water activity at 25 °C; WG, weight gain during sorption at a_W = 0.8 (g H_2O/ 100 g dry solids); W_m, monolayer content (g H_2O/ 100 g dry solids); C and K_g, constants of the Guggenheim-Anderson-de Boer (GAB) model; ζ-potential (mV); CIELAB parameters: L (lightness), a (redness-greenness), b (yellowness-blueness); WI, whiteness index; YI, yellowness index; CI, Carr's index; HR, Hausner ratio; T_g, glass transition temperature (°C); T_{onset}, onset temperature (°C) for the second degradation stage in thermogravimetric analysis (TGA); WL, weight loss (%, w.b.) in TGA.

Table 8. Main properties of blank microparticles and microcapsules.

Property	Powder	SPI-GA ratio 1-1	SPI-GA ratio 2-1	Property (cont.)	Powder	SPI-GA ratio 1-1	SPI-GA ratio 2-1
MOC	BMP	3.65^{aB}±0.01	3.93^{bB}±0.06	**b***	BMP	8.82^{aB}±0.21	9.33^{aA}±0.22
	MC	3.25^{aA}±0.03	3.43^{bA}±0.01		MC	12.72^{aA}±0.47	13.73^{aB}±0.18
$a_{W25°C}$	BMP	0.371^{aA}±0.002	0.404^{bB}±0.001	**WI**	BMP	65.40^{aB}±0.03	63.34^{bA}±1.31
	MC	0.347^{bB}±0.000	0.297^{aA}±0.001		MC	52.73^{aA}±1.97	48.53^{aB}±0.68
$WG_{0.8}$	BMP	20.753^{aB}±0.165	20.049^{bB}±0.114	**YI**	BMP	13.72^{aA}±0.02	14.60^{bA}±0.45
	MC	15.215^{aA}±0.049	14.916^{aA}±0.091		MC	20.00^{aB}±0.86	21.86^{aB}±0.32
W_m	BMP	5.207^{aB}±0.128	5.135^{bB}±0.153	**CI**	BMP	20.00^{bA}±0.00	12.87^{aA}±0.24
	MC	3.721^{aA}±0.136	3.698^{aA}±0.055		MC	35.00^{aB}±2.36	32.88^{aB}±2.99
C	BMP	11.271^{aA}±1.000	13.137^{aA}±1.535	**HR**	BMP	1.25^{bA}±0.00	1.15^{aA}±0.00
	MC	7.254^{aA}±0.770	7.618^{aA}±0.567		MC	1.54^{aB}±0.05	1.49^{aB}±0.06
K_g	BMP	0.947^{aA}±0.011	0.940^{aA}±0.009	**T_g**	BMP	173.0^{aA}±2.4	171.9^{aA}±2.5
	MC	0.949^{aA}±0.008	0.942^{aA}±0.005		MC	172.1^{aA}±3.5	169.5^{aA}±0.6
ζ-potential	BMP	-0.471^{aA}±0.014	-0.914^{bA}±0.009	**T_{onset}**	BMP	260.2^{aA}±1.9	260.8^{aA}±6.2
	MC	-0.512^{aA}±0.027	-0.744^{aA}±0.077		MC	256.6^{aA}±1.5	253.3^{aA}±3.6
L*	BMP	91.28^{aA}±0.09	91.35^{aA}±0.65	**WL**	BMP	58.63^{aA}±4.97	57.08^{aA}±2.78
	MC	90.91^{aA}±0.55	89.72^{aA}±0.13		MC	53.12^{aA}±2.31	51.71^{aA}±0.01
a*	BMP	0.04^{aA}±0.00	0.11^{bA}±0.01				
	MC	0.61^{aB}±0.04	0.53^{aB}±0.00				

SPI-GA ratio (w/w); MC, microcapsule; BMP, blank microparticle; MOC, moisture content (%, w.b.); $a_{W\ 25°C}$, water activity at 25 °C; WG, weight gain during sorption at a_W = 0,8 (g H_2O/ 100 g dry solids); W_m, monolayer content (g H_2O/ 100 g dry solids); C and K_g, constants of the Guggenheim-Anderson-de Boer (GAB) model; ζ-potential (mV); CIELAB parameters: L* (lightness), a* (redness-greenness), b* (yellowness-blueness); WI, whiteness index; YI, yellowness index; CI, Carr's index; HR, Hausner ratio; T_g, glass transition temperature (°C); T_{onset}, onset temperature (°C) for the second degradation stage in thermogravimetric analysis (TGA); WL, weight loss (%, w.b.) in TGA.

Average values (n = 3) ± standard deviation are shown.

Lower case letters in each row indicate statistically significant differences (p≤0.05) between SPI-GA ratios; capital letters indicate significant differences (p≤0.05) between blank microparticles (BMP) and microcapsules (MC).

Credit author statement

María Gabriela Bordón: conceptualization; methodology; software; validation; formal analysis; investigation; data curation; visualization; writing- original draft; writing-review & editing.

Alejandro Javier Paredes: conceptualization; methodology; investigation; validation; formal analysis.

Nahuel Matías Camacho: conceptualization; methodology; investigation; validation; formal analysis.

María Cecilia Penci: conceptualization; methodology; project administration; investigation; validation; formal analysis.

Agustín González: conceptualization; methodology; project administration; investigation; validation; formal analysis.

Santiago Daniel Palma: conceptualization; methodology; formal analysis; supervision; funding acquisition.

Pablo Daniel Ribotta: conceptualization; methodology; formal analysis; visualization; writing-original draft; writing-review & editing; supervision; funding acquisition.

Marcela Lilian Martínez: conceptualization; methodology; formal analysis; investigation; visualization; writing- original draft; writing-review & editing; project administration; funding acquisition.

Declaration of interests

☒The authors declare that they have no known competing financial interests or personal relationships that could have appeared to influence the work reported in this paper.

☐The authors declare the following financial interests/personal relationships which may be considered as potential competing interests:

Highlights

Chia oil (CO) was encapsulated by complex coacervation.

Soy protein isolate (SPI) and gum arabic (GA) were used as wall materials.

The gel strength and cross-linking were enhanced by the presence of CO in emulsions.

The monolayer content and bulk moisture diffusivity of powders were affected by CO.

Chia oil was successfully protected by microencapsulation.

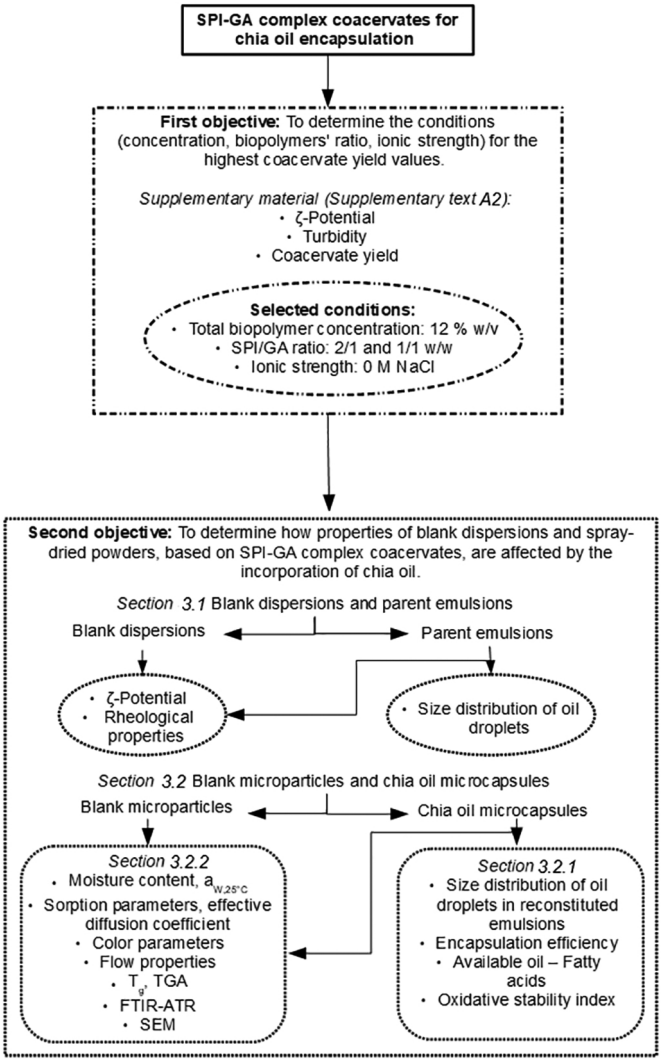
SPI-GA complex coacervates for chia oil encapsulation
First objective: To determine the conditions (concentration, biopolymers' ratio, ionic strength) for the highest coacervate yield values.
Supplementary material (Supplementary text A2):
• ζ-Potential
• Turbidity
• Coacervate yield
Selected conditions:
• Total biopolymer concentration: 12 % w/v
• SPI/GA ratio: 2/1 and 1/1 w/w
• Ionic strength: 0 M NaCl
Second objective: To determine how properties of blank dispersions and spray-dried powders, based on SPI-GA complex coacervates, are affected by the incorporation of chia oil.
Section 3.1 Blank dispersions and parent emulsions
Blank dispersions
Parent emulsions
• ζ-Potential
• Rheological properties
• Size distribution of oil droplets
Section 3.2 Blank microparticles and chia oil microcapsules
Blank microparticles
Chia oil microcapsules
Section 3.2.2
• Moisture content, $a_{W,25°C}$
• Sorption parameters, effective diffusion coefficient
• Color parameters
• Flow properties
• T_g, TGA
• FTIR-ATR
• SEM
Section 3.2.1
• Size distribution of oil droplets in reconstituted emulsions
• Encapsulation efficiency
• Available oil – Fatty acids
• Oxidative stability index

Figure 1

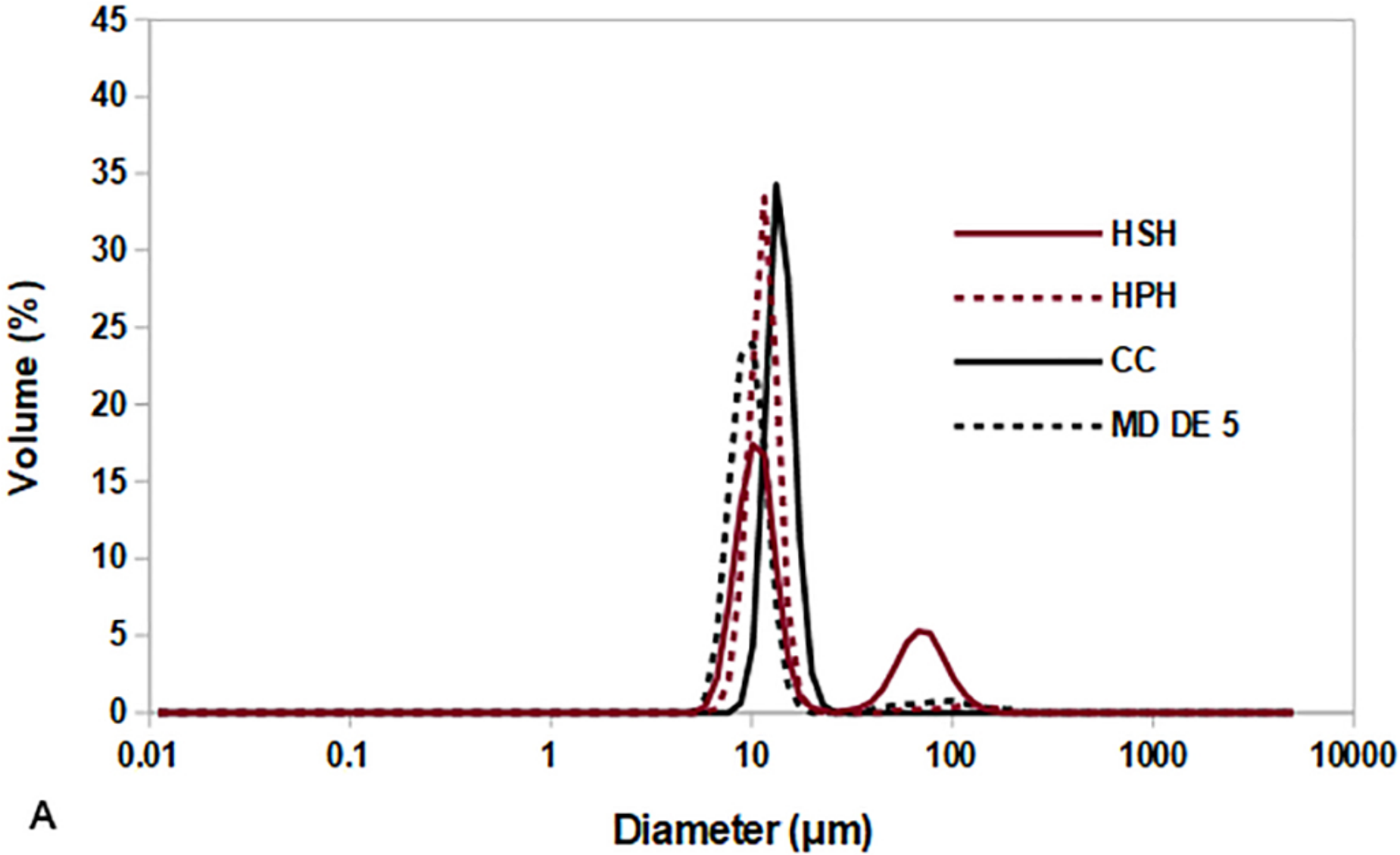
45
40
35
30
25
20
15
10
5
0
Volume (%)
0.01
0.1
1
10
100
1000
10000
Diameter (µm)
HSH
HPH
CC
MD DE 5
A

Figure 2A

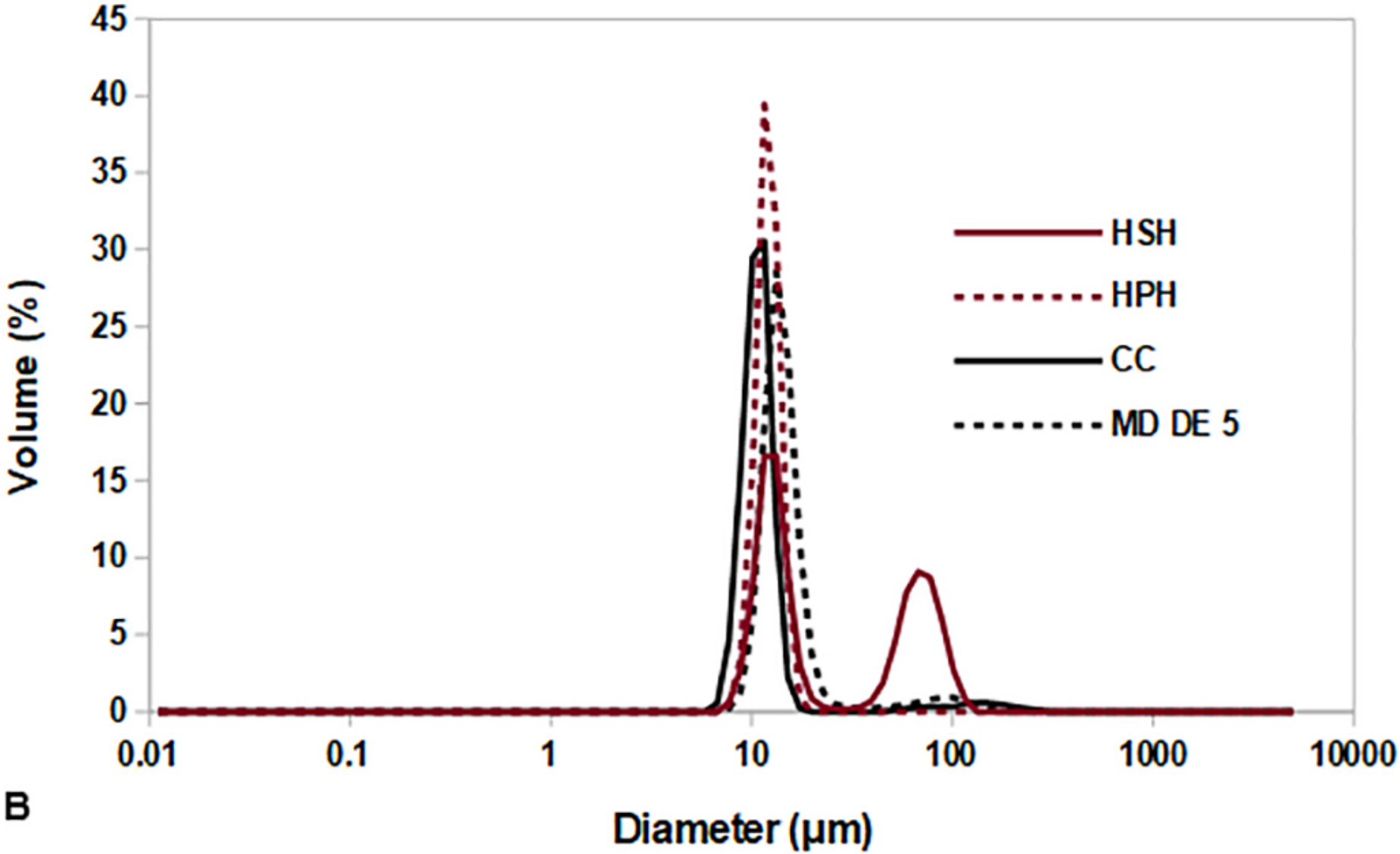
45
40
35
30
25
20
15
10
5
0
Volume (%)
0.01
0.1
1
10
100
1000
10000
Diameter (µm)
HSH
HPH
CC
MD DE 5
B

Figure 2B

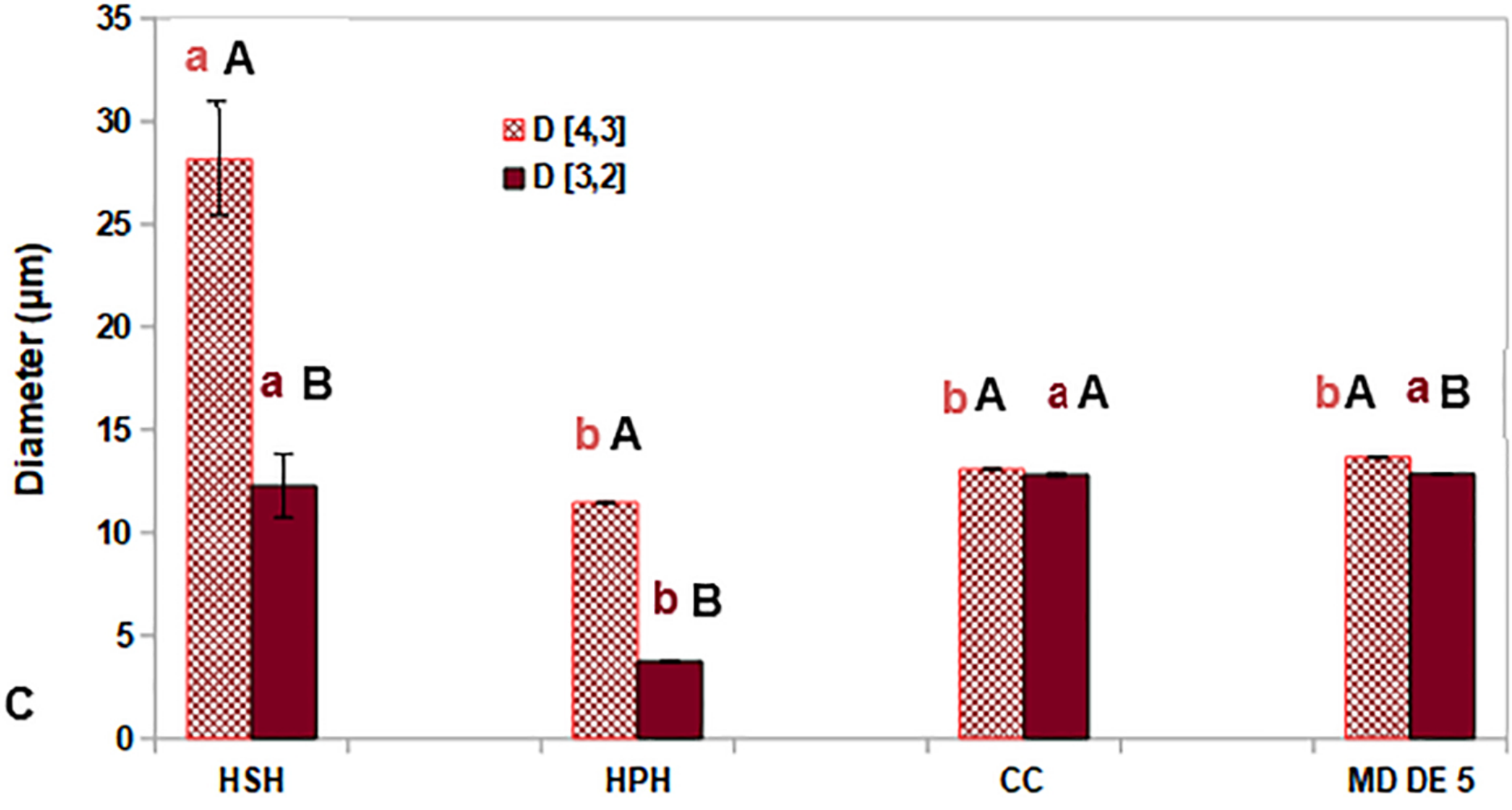
C
Diameter (µm)
35
30
25
20
15
10
5
0
D [4,3]
D [3,2]
a A
a B
b A
b B
b A
a A
b A
a B
HSH
HPH
CC
MD DE 5

Figure 2C

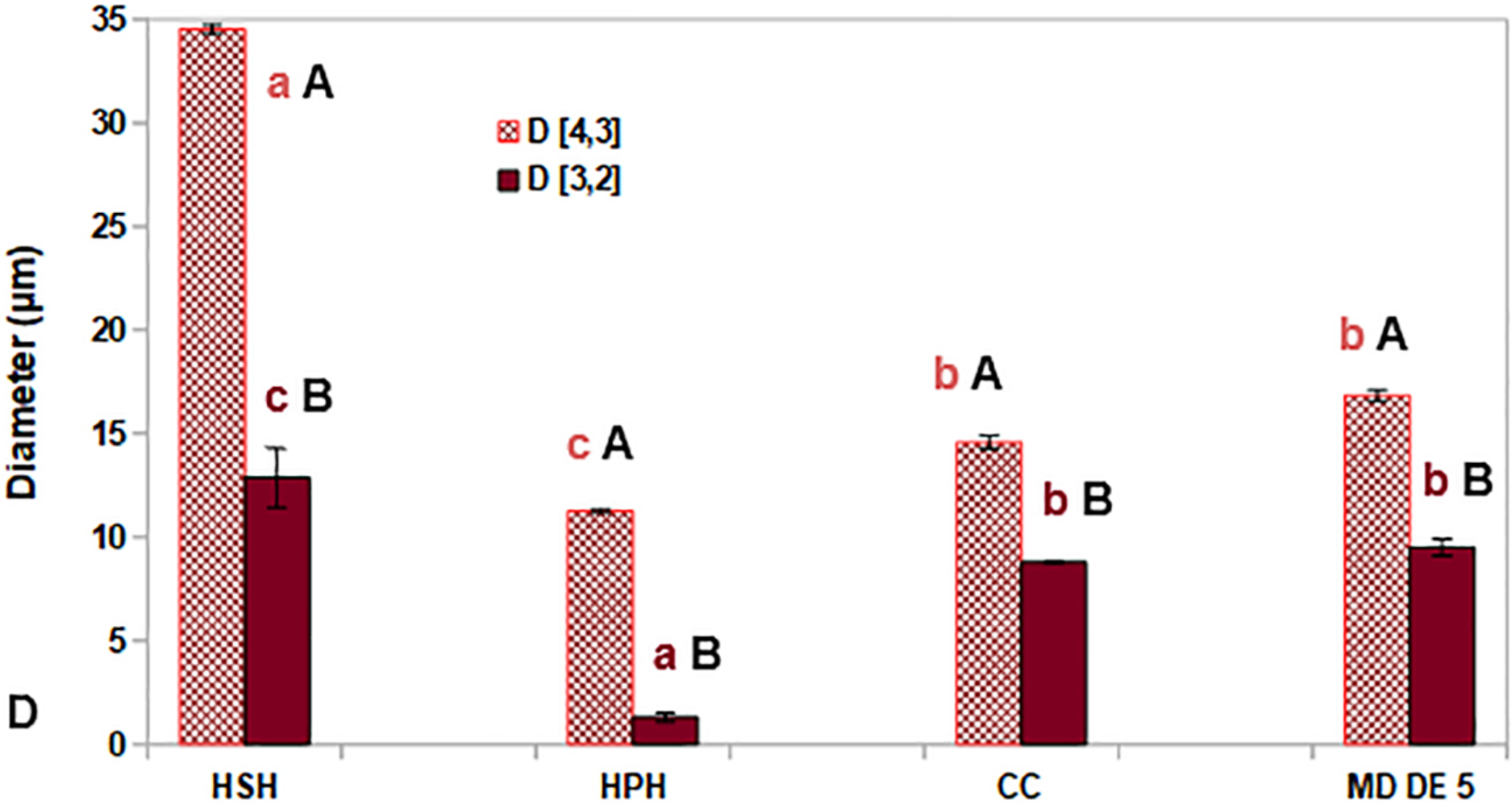
Diameter (µm)
35
30
25
20
15
10
5
0
D [4,3]
D [3,2]
a A
c B
c A
a B
b A
b B
b A
b B
HSH
HPH
CC
MD DE 5
D

Figure 2D

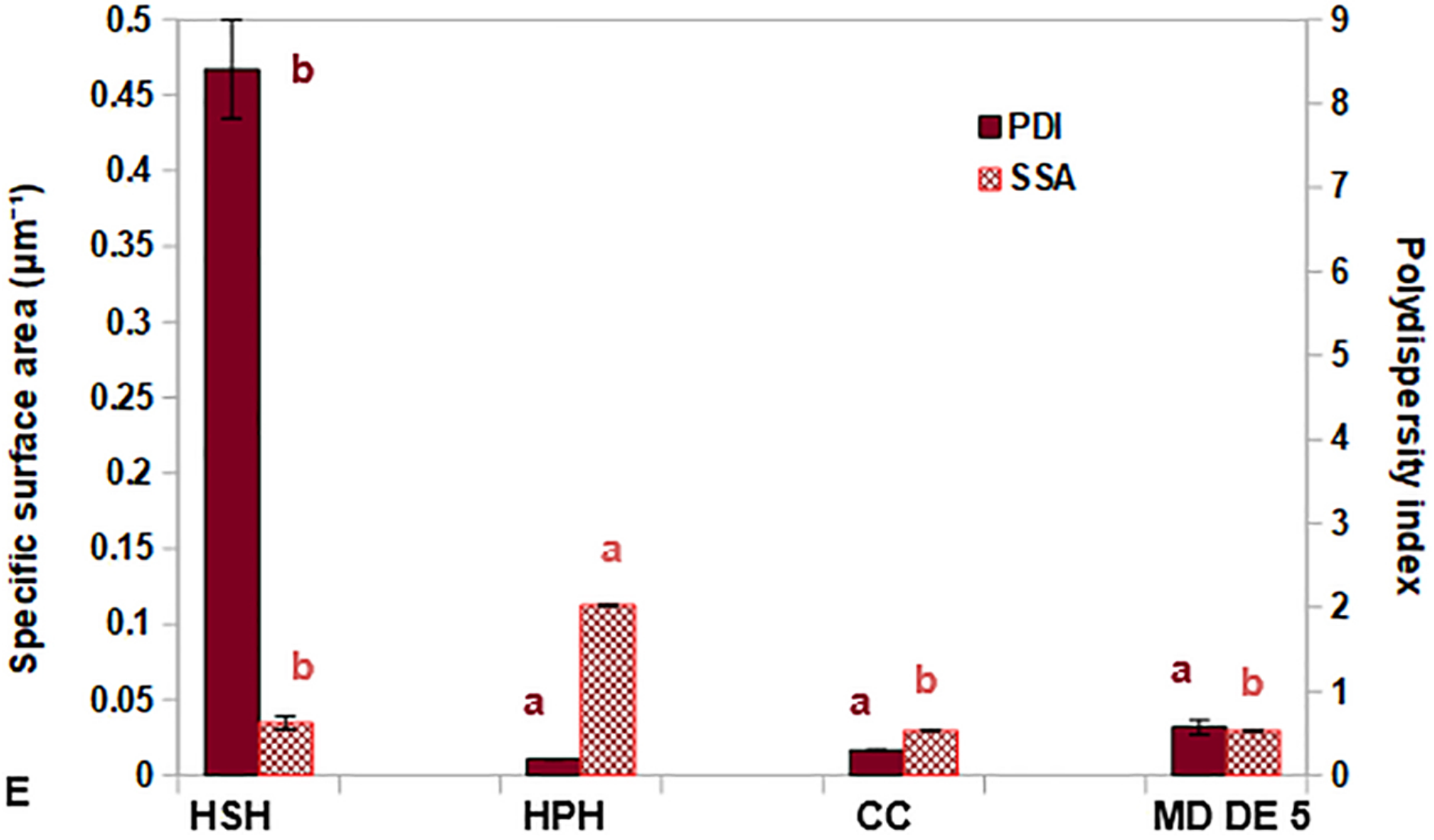
Specific surface area (µm⁻¹)
Polydispersity index
PDI
SSA
0.5
0.45
0.4
0.35
0.3
0.25
0.2
0.15
0.1
0.05
0
9
8
7
6
5
4
3
2
1
0
b
b
a
a
a
b
a
b
HSH
HPH
CC
MD DE 5

Figure 2E

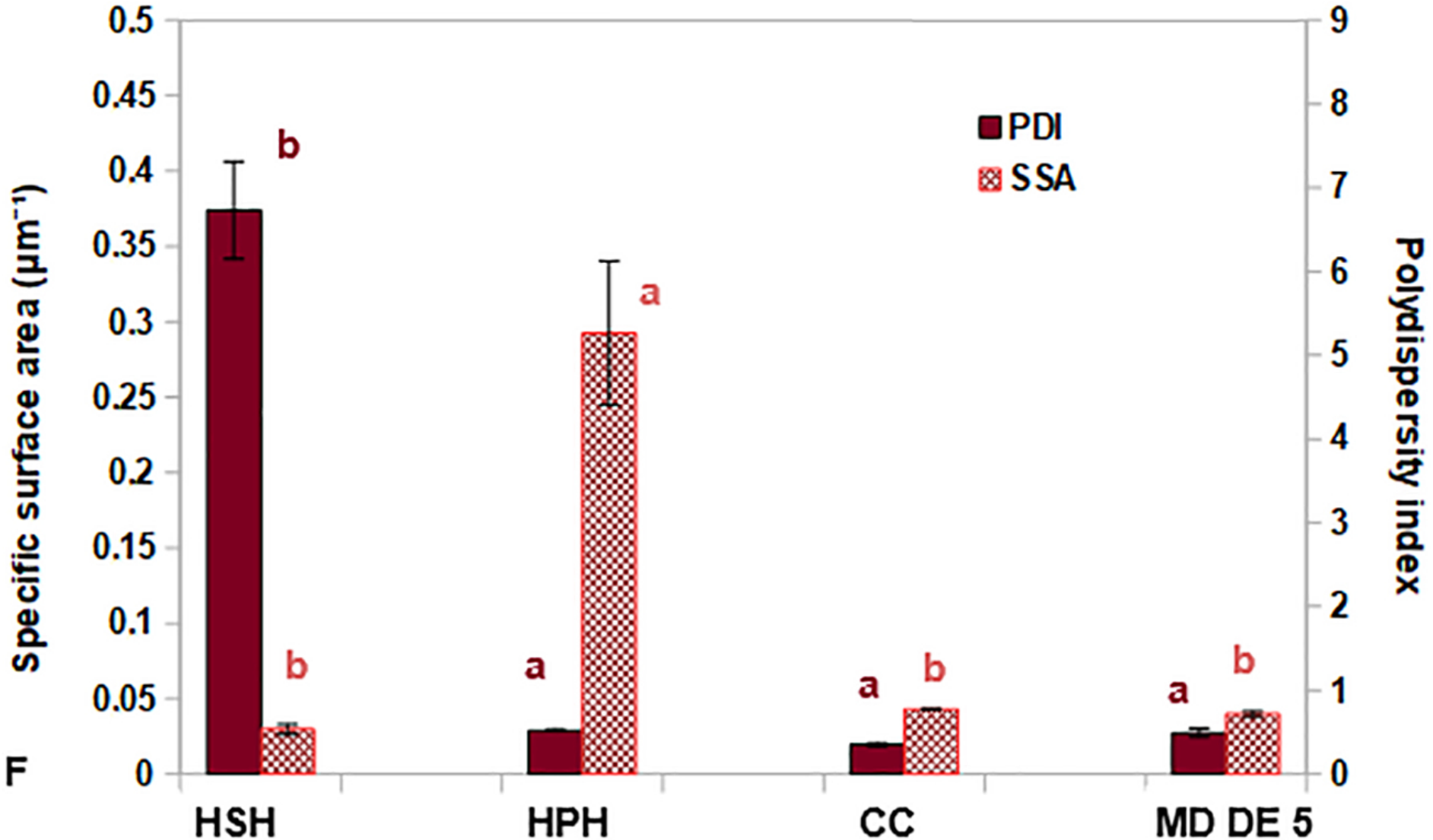
Specific surface area (µm⁻¹)
Polydispersity index
PDI
SSA
0.5
0.45
0.4
0.35
0.3
0.25
0.2
0.15
0.1
0.05
0
9
8
7
6
5
4
3
2
1
0
b
b
a
a
a
b
a
b
HSH
HPH
CC
MD DE 5

Figure 2F

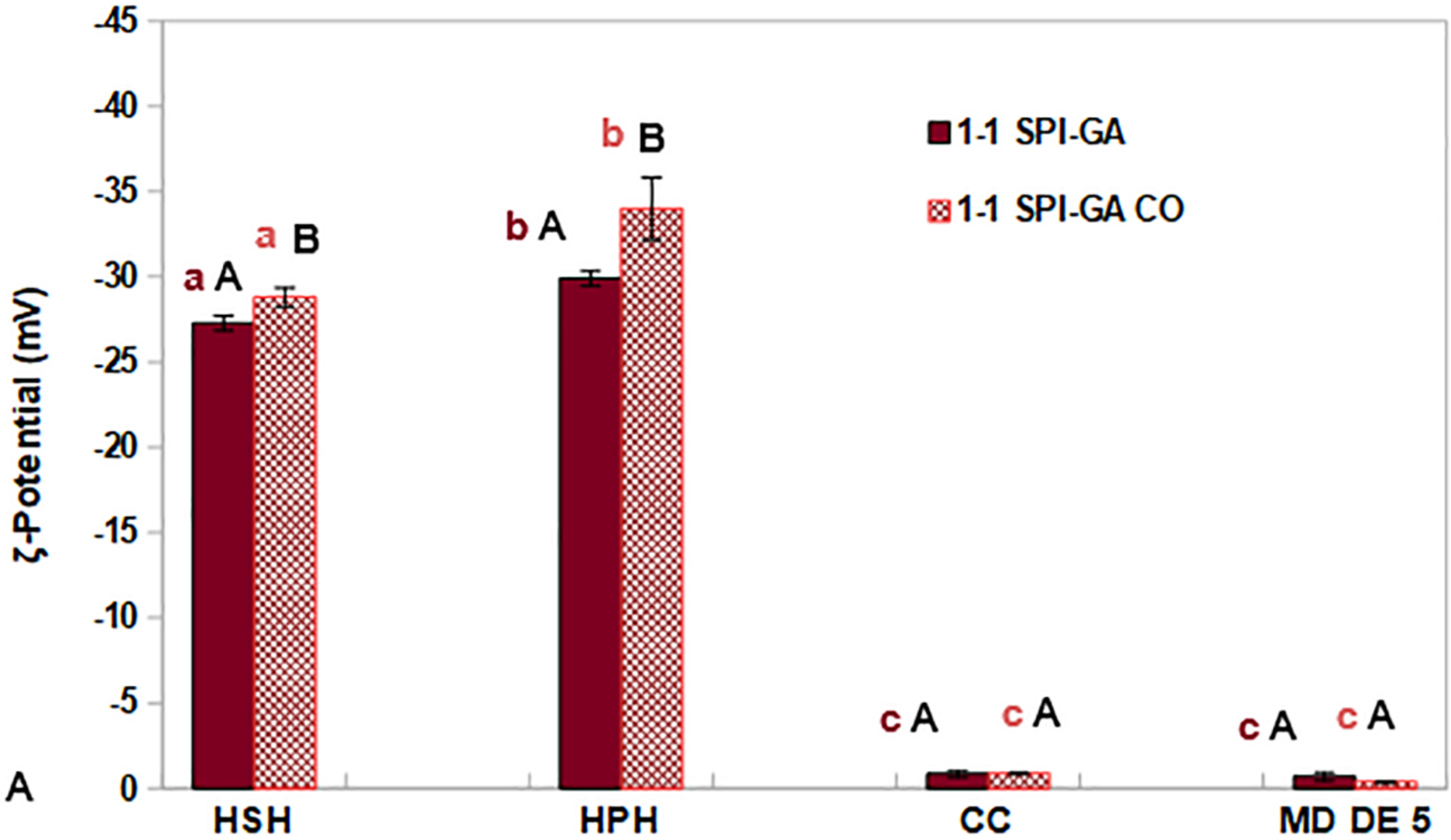
A
ζ-Potential (mV)
-45
-40
-35
-30
-25
-20
-15
-10
-5
0
a A
a B
b A
b B
c A
c A
c A
c A
1-1 SPI-GA
1-1 SPI-GA CO
HSH
HPH
CC
MD DE 5

Figure 3A

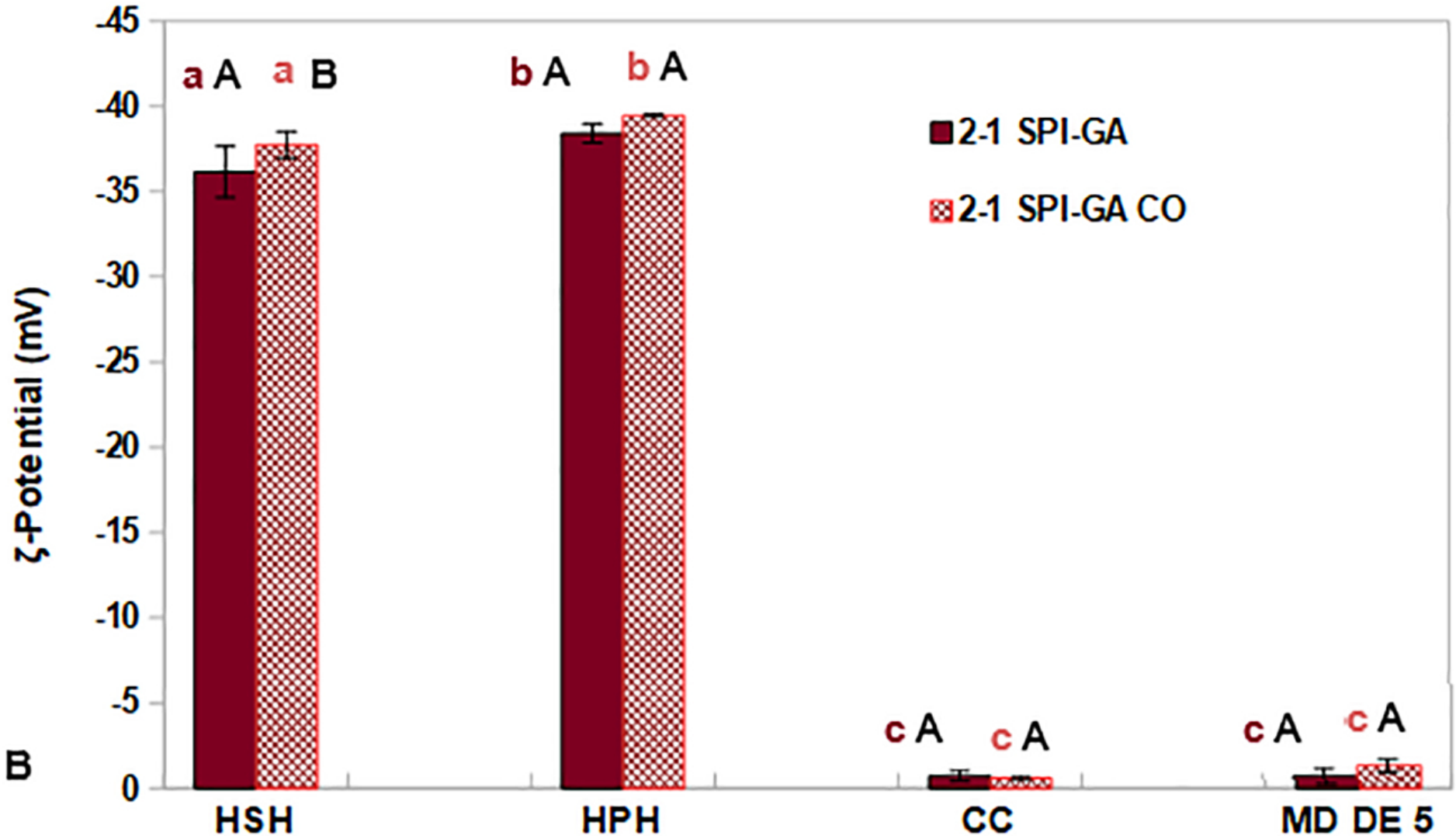
B
ζ-Potential (mV)
-45
-40
-35
-30
-25
-20
-15
-10
-5
0
a A
a B
b A
b A
c A
c A
c A
c A
2-1 SPI-GA
2-1 SPI-GA CO
HSH
HPH
CC
MD DE 5

Figure 3B

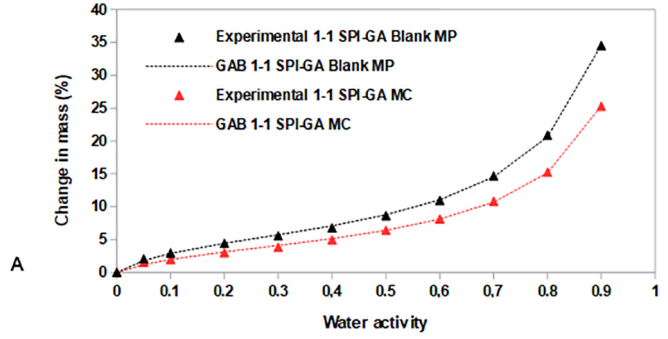
Experimental 1-1 SPI-GA Blank MP
GAB 1-1 SPI-GA Blank MP
Experimental 1-1 SPI-GA MC
GAB 1-1 SPI-GA MC
Change in mass (%)
Water activity
A

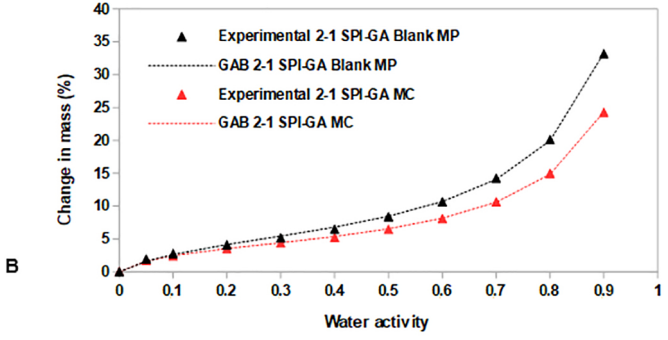
Experimental 2-1 SPI-GA Blank MP
GAB 2-1 SPI-GA Blank MP
Experimental 2-1 SPI-GA MC
GAB 2-1 SPI-GA MC
Change in mass (%)
Water activity
B

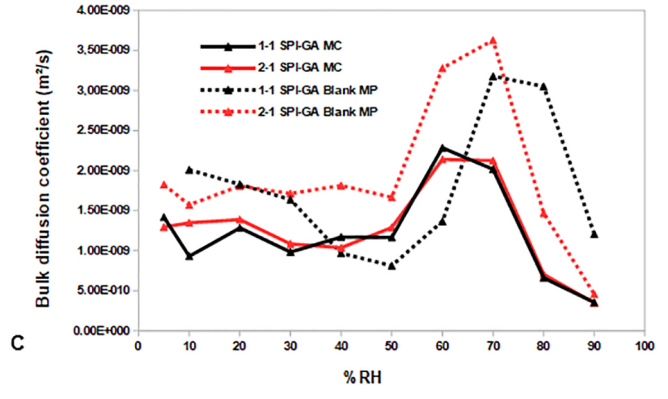
1-1 SPI-GA MC
2-1 SPI-GA MC
1-1 SPI-GA Blank MP
2-1 SPI-GA Blank MP
Bulk diffusion coefficient (m²/s)
% RH
C

Figure 4

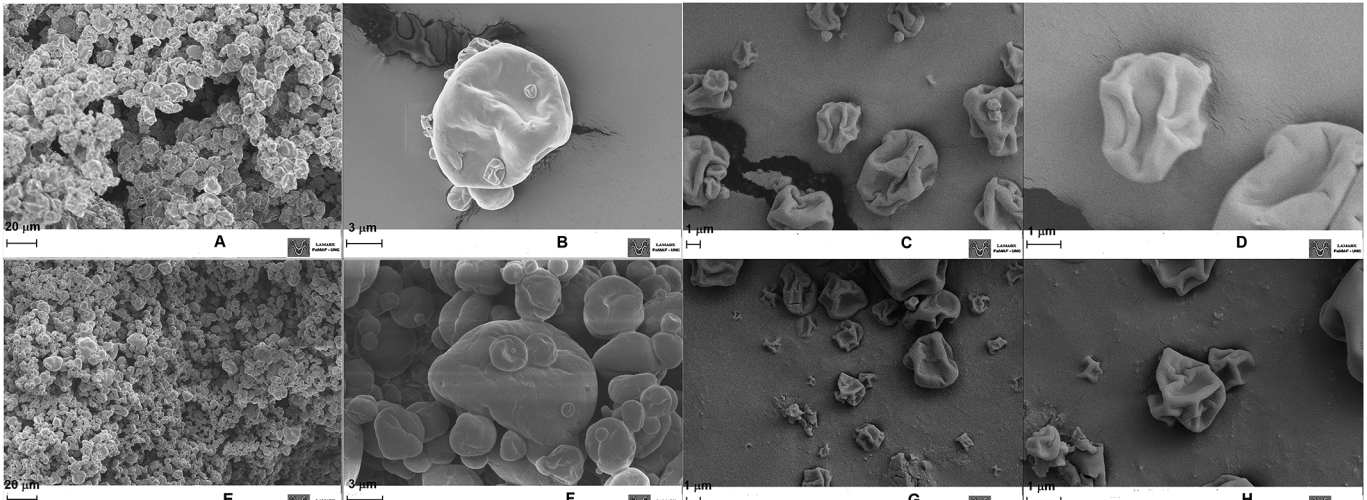

Figure 5